Journal of Computational Physics 228 (2009) 8779–8806

Contents lists available at ScienceDirect

Journal of Computational Physics

journal homepage: www.elsevier.com/locate/jcp

A new time–space domain high-order finite-difference method for the acoustic wave equation

Yang Liu [a,b,*], Mrinal K. Sen [b]

[a] State Key Laboratory of Petroleum Resource and Prospecting, China University of Petroleum, Changping, Beijing 102249, PR China
[b] The Institute for Geophysics, John A. and Katherine G. Jackson School of Geosciences, The University of Texas at Austin, 10100 Burnet Road, R2200 Austin, TX 78758, USA

ARTICLE INFO

Article history:
Received 1 June 2009
Received in revised form 26 August 2009
Accepted 27 August 2009
Available online 3 September 2009

Keywords:
Time–space domain
Finite-difference
Dispersion relation
Plane wave theory
Second-order spatial derivatives
Arbitrary-order accuracy
Acoustic wave equation
Dispersion analysis
Stability condition
Numerical modeling
Optimal finite-difference stencil length
Staggered-grid finite-difference

ABSTRACT

A new unified methodology was proposed in Finkelstein and Kastner (2007) [39] to derive spatial finite-difference (FD) coefficients in the joint time–space domain to reduce numerical dispersion. The key idea of this method is that the dispersion relation is completely satisfied at several designated frequencies. We develop this new time–space domain FD method further for 1D, 2D and 3D acoustic wave modeling using a plane wave theory and the Taylor series expansion. New spatial FD coefficients are frequency independent though they lead to a frequency dependent numerical solution. We prove that the modeling accuracy is 2nd-order when the conventional $(2M)$th-order space domain FD and the 2nd-order time domain FD stencils are directly used to solve the acoustic wave equation. However, under the same discretization, the new 1D method can reach $(2M)$th-order accuracy and is always stable. The 2D method can reach $(2M)$th-order accuracy along eight directions and has better stability. Similarly, the 3D method can reach $(2M)$th-order accuracy along 48 directions and also has better stability than the conventional FD method. The advantages of the new method are also demonstrated by the results of dispersion analysis and numerical modeling of acoustic wave equation for homogeneous and inhomogeneous acoustic models. In addition, we study the influence of the FD stencil length on numerical modeling for 1D inhomogeneous media, and derive an optimal FD stencil length required to balance the accuracy and efficiency of modeling. A new time–space domain high-order staggered-grid FD method for the 1D acoustic wave equation with variable densities is also developed, which has similar advantages demonstrated by dispersion analysis, stability analysis and modeling experiments. The methodology presented in this paper can be easily extended to solve similar partial difference equations arising in other fields of science and engineering.

1. Introduction

Finite-difference (FD) methods have been widely used in seismic modeling (e.g. [1–4]) and seismic migration (e.g. [5–8]) since these methods are fairly easy to implement. They also require relatively small memory and computation time compared to other purely numerical methods such as finite elements (e.g. [9]) and modified direct solution methods (DSM) [49,50]. A 2nd-order FD scheme is usually used for approximating temporal derivatives to perform wave field recursion

* Corresponding author. Address: State Key Laboratory of Petroleum Resource and Prospecting, China University of Petroleum, Changping, Beijing 102249, PR China..
E-mail addresses: wliuyang@vip.sina.com (Y. Liu), mrinal@ig.utexas.edu (M.K. Sen).

0021-9991/$ - see front matter © 2009 Elsevier Inc. All rights reserved.
doi:10.1016/j.jcp.2009.08.027

effectively and stably; this, however, limits the accuracy of modeling. A smaller time step or grid size may increase the modeling precision but will require more computation time. Many methods, such as high-order, staggered-grid and implicit methods, have been developed to improve the accuracy which do not markedly increase the computation cost.

High-order FD on the space derivatives is a popular method to increase modeling accuracy (e.g. [10–19]). A low-order FD algorithm uses a shorter operator but needs more grid points for discretization. A high-order FD algorithm uses a longer operator but needs fewer grid points. It has been demonstrated that high-order FD schemes have practical advantages when applied to the scalar wave equation [10]. The FD schemes with accuracy of any or all orders have been derived for the first-order derivatives and used to solve wave equations (e.g. [10,11]). FD coefficients are generally determined by a Taylor series expansion (e.g. [10,43]) or by optimization (e.g. [11,44–46,48,51,52]). The effect of reducing the formal order of accuracy of a FD scheme in order to optimize its high-wavenumber performance was investigated [47] using the 1D nonlinear unsteady inviscid Burgers' equation and it was found that the benefits of optimization do carry over into nonlinear applications. FD operators, accounting explicitly for the amplitude spectrum, give more accurate results than Taylor or optimum operators in the elastic wave equation modeling [45]. The modified FD operators were derived by optimally minimizing the numerical dispersion of P- and S-velocities as an indirect consequence of their minimizing the error of synthetic seismograms, and the accuracy of synthetic seismograms computed using the modified operators was greatly improved as compared to conventional FD operators [51]. Using the Taylor expansion, the FD method with any even-order accuracy has been developed for arbitrary-order derivatives [14] and utilized to simulate wave propagation in two-phase anisotropic media [19].

Compared with conventional-grid FD methods, staggered-grid FD methods have greater precision and better stability and have been widely used in seismic modeling. An initial work for modeling of elastic wave equations was reported in [20]. A second-order velocity-stress staggered FD schemes for modeling SH-wave and P-SV wave propagation in generally heterogeneous media was proposed [21,22]. This method was used to simulate elastic wave propagation in 3D media (e.g. [23–28]). When the medium possesses discontinuities with large contrasts, modeling of elastic waves with an explicit FD scheme on a staggered grid causes instability problems. Rotated staggered grids, where all the medium parameters are defined at appropriate positions within an elementary cell for the essential operations, have also been used in the FD method [29–32].

Implicit FD methods have also been developed to improve the modeling accuracy. There are two kinds of implicit method. One is the implicit FD on temporal derivatives for the elastic wave equations [33]. It expresses a temporal derivative value at some point at a future time in terms of the values of the variable at that point and at its neighboring points at present time, past times, and future times. The implicit method for temporal derivatives has been used successfully in seismic migration algorithms [34]. The other implicit method is the implicit FD on spatial derivatives (e.g. [41,42]). This method expresses the spatial derivative value at some point in terms of the function values at that point and at its neighboring points and the derivative values at its neighboring points. A compact FD method [2] is such an implicit method, which has been widely applied in modeling (e.g. [35–38]).

Since the explicit high-order FD on temporal derivatives is usually unstable in the wave equation modeling (e.g. [17]), spatial derivatives are used to replace high-order temporal derivatives (e.g. [10,17]) to increase the accuracy of temporal derivatives with additional computational cost. Our goal is to derive new FD coefficients for spatial derivatives that can increase the accuracy of acoustic wave modeling without increasing calculation amount. Generally, most FD methods determine the FD stencils for spatial derivatives only in the space domain. However, the seismic wave propagation calculation is done both in space and time domains. If these stencils are directly used to solve the wave equations, the dispersion will always exist and may be very large. To address this issue, a unified methodology in [39] has been proposed to derive the FD coefficients in the joint time–space domain. The key idea of this method is that the dispersion relation is completely satisfied at designated frequencies; thus several equations are formed and the FD coefficients are obtained by solving these equations. Thus one can obtain dispersion free simulation at a given frequency. However, since different frequencies require different dispersion criterion, this method may not be very useful in practical applications which require time domain simulation where the source spectrum contains a continuous band of frequencies. This FD method was developed further for the 1D lossless and boundless wave equation in [40] and its spatial FD coefficients were determined at one designated frequency to obtain arbitrary-order accuracy.

In this paper, we develop a unified methodology similar to the method [39,40] and employ the Taylor series expansion of dispersion relation to derive the FD coefficients in the joint time–space domain. We prove that the modeling accuracy is of 2nd-order when the conventional $(2M)$th-order space domain FD and the 2nd-order time domain FD stencils are directly used to solve the acoustic wave equation. The new spatial FD coefficients for the 1D acoustic wave equation modeling are determined by the Courant number and the space point number and are independent of frequency. We demonstrate that while spatial difference coefficients of 1D in [39] depend on the space point number, the Courant number and frequencies, our difference coefficients for space derivatives are determined by the space point number and the Courant number only. For the 1D modeling, the accuracy can be improved from 2nd-order of the conventional method to $(2M)$th-order of the new method when $2M+1$ points are involved in the spatial derivatives and 3 points in the temporal derivatives. This conclusion can be obtained from [40]. Equations for solving 1D spatial FD coefficients derived in our paper are equivalent to those in [40]. However, we derive their explicit expressions for the first time. For 2D modeling, spatial difference coefficients in [39] depend on the space point number, the Courant number, frequencies and angles. Our difference coefficients for space derivatives in 2D are determined by the space point number, the Courant number and the angle. Moreover, we find an optimal angle $\pi/8$ which enables the modeling to reach $(2M)$th-order accuracy along eight directions; therefore, our difference coefficients are independent of angle. For the new 3D method, $(2M)$th-order accuracy can be reached along 48 directions

also. The advantages of the new 1D and 2D methods are demonstrated by dispersion analysis, stability analysis and numerical modeling. In addition, we study the influence of FD stencil length on numerical modeling for inhomogeneous media, and the optimal FD stencil length to balance the modeling accuracy and efficiency. We also develop a new time–space domain high-order staggered-grid FD method for the acoustic wave equation where the density is inside a partial derivative. Note that although the FD coefficients derived from time–space domain dispersion relations in this paper are frequency independent, they still lead to frequency dependent solution.

The structure of this paper is as follows. First, we analyze the accuracy of the conventional FD stencils for the acoustic wave equation. Then, we derive equations for solving new spatial FD coefficients. Dispersion and stability analyses are carried out for both the conventional and the new methods. Numerical modeling both in homogeneous and inhomogeneous media are performed and compared for the conventional and the new methods. In the discussion section, we discuss the influence of FD stencil length and choice of an optimal FD stencil length and develop a new time–space domain high-order staggered-grid FD method for the acoustic wave equation with variable densities. Finally, we draw conclusions based on these analyses.

2. Accuracy analysis of conventional FD stencils for acoustic wave equations

We start our analysis with the constant density 1D acoustic wave equation or scalar wave equation in homogenous media given by

$$\frac{\partial^2 p}{\partial x^2} = \frac{1}{v^2}\frac{\partial^2 p}{\partial t^2}, \tag{1}$$

where $p = p(x,t)$ is a scalar wave field, and v is the velocity.

Generally, an explicit high-order FD on temporal derivatives requires large computer memory and is usually unstable (e.g. [17]), the following 2nd-order FD is usually used,

$$\frac{\partial^2 p}{\partial t^2} \approx \frac{\delta^2 p}{\delta t^2} = \frac{1}{\tau^2}\left[-2p_0^0 + \left(p_0^{-1} + p_0^1\right)\right], \tag{2}$$

where

$$p_m^n = p(x + mh, t + n\tau), \tag{3}$$

h is the grid size, τ is the time step. Generally, the modeling accuracy is improved by using a high-order FD on spatial derivatives; a $(2M)$th-order FD formula is given by

$$\frac{\partial^2 p}{\partial x^2} \approx \frac{\delta^2 p}{\delta x^2} = \frac{1}{h^2}\left[a_0 p_0^0 + \sum_{m=1}^{M} a_m\left(p_{-m}^0 + p_m^0\right)\right]. \tag{4}$$

Substituting Eqs. (2) and (4) into (1) and rearranging it, we have

$$a_0 p_0^0 + \sum_{m=1}^{M} a_m\left(p_{-m}^0 + p_m^0\right) \approx \frac{h^2}{v^2\tau^2}\left[\left(p_0^{-1} + p_0^1\right) - 2p_0^0\right]. \tag{5}$$

Note that in the conventional method, the FD coefficients on spatial derivatives are determined in the space domain alone. Using the plane wave theory, we let

$$p_m^n = e^{\mathrm{i}[k(x+mh)-\omega(t+n\tau)]} = e^{\mathrm{i}(kx-\omega t)}e^{\mathrm{i}(mkh-n\omega\tau)}, \tag{6}$$

where k is the wavenumber, ω is the angular frequency, $\mathrm{i} = \sqrt{-1}$. Substituting Eq. (6) into (4) and simplifying it, we have

$$-k^2 \approx \frac{1}{h^2}\left[a_0 + 2\sum_{m=1}^{M} a_m \cos(mkh)\right]. \tag{7}$$

Using the Taylor series expansion for cosine functions, we obtain

$$-k^2 \approx \frac{a_0}{h^2} + \frac{2}{h^2}\sum_{m=1}^{M} a_m\left[1 + \sum_{j=1}^{\infty}(-1)^j\frac{(mhk)^{2j}}{(2j)!}\right]. \tag{8}$$

By comparing the coefficients of $k^0, k^2, \ldots, k^{2M}$, $M+1$ equations can be obtained to solve for FD coefficients $a_0, a_1, \ldots, a_M$ [14,19]. Then, the error of the FD on the spatial derivatives is derived from Eq. (8) as follows:

$$\frac{2}{h^2}\sum_{m=1}^{M} a_m\left[\sum_{j=M+1}^{\infty}(-1)^j\frac{(mhk)^{2j}}{(2j)!}\right]. \tag{9}$$

Therefore, we obtain the following equation

$$\frac{1}{h^2}\left[a_0+2\sum_{m=1}^{M}a_m\cos(mkh)\right]=-k^2+\frac{2}{h^2}\sum_{j=M+1}^{\infty}\left[(-1)^j\sum_{m=1}^{M}a_m\frac{(mhk)^{2j}}{(2j)!}\right]. \tag{10}$$

Similarly, we obtain

$$\frac{1}{\tau^2}[-2+2\cos(\omega\tau)]=-\omega^2+\frac{2}{\tau^2}\left[\sum_{j=2}^{\infty}(-1)^j\frac{(\omega\tau)^{2j}}{(2j)!}\right]. \tag{11}$$

When 1D space domain and time domain FD formulas are directly used to solve the 1D acoustic wave equation, the absolute error can be obtained from Eq. (1) by using Eqs. (2), (4) and (6),

$$\varepsilon=\left|\frac{1}{h^2}\left[a_0+2\sum_{m=1}^{M}a_m\cos(mkh)\right]-\frac{1}{v^2\tau^2}[-2+2\cos(\omega\tau)]\right|. \tag{12}$$

Substituting Eqs. (10) and (11) and $v=\omega/k$ into Eq. (12), we have

$$\varepsilon=\left|2\sum_{j=M+1}^{\infty}\left[(-1)^j\sum_{m=1}^{M}a_m\frac{m^{2j}k^{2j}}{(2j)!}h^{2j-2}\right]-2\sum_{j=2}^{\infty}\left[(-1)^j\frac{r^{2j-2}k^{2j}}{(2j)!}h^{2j-2}\right]\right|, \tag{13}$$

where

$$r=\frac{v\tau}{h}. \tag{14}$$

Since the minimum power of h in the error function (13) is 2, the FD accuracy is 2nd-order. Therefore, when we use the $(2M)$th-order space domain FD and the 2nd-order time domain FD stencils to solve the 1D acoustic wave equation, the accuracy is of 2nd-order. It is fairly obvious that the conclusion is the same for 2D and 3D acoustic wave equations. It is worthwhile to note that increasing M may decrease the magnitude of FD errors but may not increase the order of accuracy. The main reason is that the FD stencils are designed in the space and time domains, respectively, but the wave equation must be solved in both the space and the time domains simultaneously.

3. Time–space domain high-order FD method for acoustic wave equations

Here, we propose a new FD scheme by determining the coefficients for the spatial derivatives in the joint time–space domain following some novel ideas outlined in [39]. However, the details of our approach are different in that we derive coefficients that are better suited to modeling in time domain comprising a continuous spectrum of frequencies. In our paper, the spatial and temporal derivatives are treated separately first, and then combined using the wave equation, whereas in [40] both derivatives for the 1D wave equation are approximated concurrently while already embedded in the equation.

3.1. 1D acoustic wave equation

The method in [39] was proposed to derive the FD coefficients in the joint time–space domain. The key idea of this method is that the dispersion relation is completely satisfied at designated frequencies; thus several equations are formed and the FD coefficients are obtained by solving these equations. It is obvious that different designated frequencies give different FD coefficients. Since the source spectrum contains a continuous band of frequencies, our method determines the FD coefficients by using the Taylor series expansion in the dispersion relation. Our FD coefficients of 1D are, however, equivalent to those in [40]. The details of our derivation are outlined below.

Substituting Eqs. (6) and (14) into (5) and simplifying it, we obtain

$$a_0+2\sum_{m=1}^{M}a_m\cos(mkh)\approx 2r^{-2}[\cos(rkh)-1]. \tag{15}$$

Using the Taylor series expansion for cosine functions, we have

$$a_0+2\sum_{m=1}^{M}a_m\left[1+\sum_{j=1}^{\infty}(-1)^j\frac{(mkh)^{2j}}{(2j)!}\right]\approx 2r^{-2}\left[\sum_{j=1}^{\infty}(-1)^j\frac{(rkh)^{2j}}{(2j)!}\right]. \tag{16}$$

Comparing coefficients of k^{2j}, we obtain

$$a_0+2\sum_{m=1}^{M}a_m=0, \tag{17a}$$

$$\sum_{m=1}^{M}m^{2j}a_m=r^{2j-2}\quad(j=1,2,\ldots,M). \tag{17b}$$

Eqs. (17a) and (17b) are equivalent to Eqs. (15a) and (15b) in [40]. We can rewrite Eq. (17b) as the following matrix form

$$\begin{bmatrix} 1^0 & 2^0 & \cdots & M^0 \\ 1^2 & 2^2 & \cdots & M^2 \\ \vdots & \vdots & \vdots & \vdots \\ 1^{2M-2} & 2^{2M-2} & \cdots & M^{2M-2} \end{bmatrix} \begin{bmatrix} 1^2 a_1 \\ 2^2 a_2 \\ \vdots \\ M^2 a_M \end{bmatrix} = \begin{bmatrix} 1 \\ r^2 \\ \vdots \\ r^{2M-2} \end{bmatrix}. \tag{18}$$

The coefficient matrix of Eq. (18) is a Vandermonde matrix. Solving these equations, we obtain

$$a_m = \frac{\prod_{1\leqslant n<m}(r^2-n^2)\prod_{m<n\leqslant M}(n^2-r^2)}{m^2\prod_{1\leqslant n<m}(m^2-n^2)\prod_{m<n\leqslant M}(n^2-m^2)} \quad (m=1,2,\ldots,M). \tag{19}$$

Since it is necessary that $r \leqslant 1$ in the numerical modeling, Eq. (19) can be rewritten as

$$a_m = \frac{(-1)^{m+1}}{m^2} \prod_{1\leqslant n\leqslant M, n\neq m} \left|\frac{n^2-r^2}{n^2-m^2}\right|. \tag{20}$$

The coefficient a_0 can be calculated by Eq. (17a). When $r = 0$, the FD coefficients are the same as those of the conventional method (see in [14,19]). That is, the conventional method is just a special case of the new method.

The error function of Eq. (12) can be rewritten as follows:

$$\varepsilon = \left|\frac{1}{h^2}\left[a_0 + 2\sum_{m=1}^{M} a_m \cos(mkh) - \frac{2}{r^2}(\cos(rkh)-1)\right]\right|. \tag{21}$$

Using Eqs. (16), (17a) and (17b), we have

$$\varepsilon = \left|\frac{2}{h^2}\sum_{m=1}^{M} a_m\left[\sum_{j=M+1}^{\infty}(-1)^j\frac{(mkh)^{2j}}{(2j)!}\right] - \frac{2}{h^2}r^{-2}\left[\sum_{j=M+1}^{\infty}(-1)^j\frac{(rkh)^{2j}}{(2j)!}\right]\right| = \left|\sum_{j=M+1}^{\infty}\frac{2(-1)^j}{(2j)!}\left(\sum_{m=1}^{M} m^{2j}a_m - r^{2j-2}\right)k^{2j}h^{2j-2}\right|. \tag{22}$$

This is the error function of this new method. Since the minimum power of h in the error function (22) is $2M$, the accuracy of FD is of $(2M)$th-order.

3.2. 2D acoustic wave equation

The 2D acoustic wave equation is

$$\frac{\partial^2 p}{\partial x^2} + \frac{\partial^2 p}{\partial z^2} = \frac{1}{v^2}\frac{\partial^2 p}{\partial t^2}. \tag{23}$$

Since the same FD is usually used for spatial derivatives, we let

$$\frac{\partial^2 p}{\partial x^2} \approx \frac{\delta^2 p}{\delta x^2} = \frac{1}{h^2}\left[a_0 p^0_{0,0} + \sum_{m=1}^{M} a_m\left(p^0_{-m,0} + p^0_{m,0}\right)\right], \tag{24a}$$

$$\frac{\partial^2 p}{\partial z^2} \approx \frac{\delta^2 p}{\delta z^2} = \frac{1}{h^2}\left[a_0 p^0_{0,0} + \sum_{m=1}^{M} a_m\left(p^0_{0,-m} + p^0_{0,m}\right)\right], \tag{24b}$$

where

$$p^n_{m,j} = p(x+mh, z+jh, t+n\tau). \tag{25}$$

The 2nd-order FD stencil for the temporal derivative is

$$\frac{\partial^2 p}{\partial t^2} \approx \frac{\delta^2 p}{\delta t^2} = \frac{1}{\tau^2}\left[-2p^0_{0,0} + \left(p^{-1}_{0,0} + p^1_{0,0}\right)\right]. \tag{26}$$

Using Eqs. (24a), (24b) and (26), Eq. (23) is changed as follows:

$$\frac{1}{h^2}\left[2a_0 p^0_{0,0} + \sum_{m=1}^{M} a_m\left(p^0_{-m,0} + p^0_{m,0} + p^0_{0,-m} + p^0_{0,m}\right)\right] \approx \frac{1}{v^2\tau^2}\left[-2p^0_{0,0} + \left(p^{-1}_{0,0} + p^1_{0,0}\right)\right]. \tag{27}$$

Let

$$p^n_{m,j} = e^{\mathrm{i}[k_x(x+mh)+k_z(z+jh)-\omega(t+n\tau)]}. \tag{28}$$

Substituting Eq. (28) into (27) and simplifying it, we obtain

$$a_0 + \sum_{m=1}^{M} a_m[\cos(mk_x h) + \cos(mk_z h)] \approx r^{-2}[-1 + \cos(\omega\tau)]. \tag{29}$$

Let

$$k_x = k\cos\theta, \quad k_z = k\sin\theta, \tag{30}$$

where θ is the propagation direction angle of plane wave. Then Eq. (29) can be written as

$$a_0 + \sum_{m=1}^{M} a_m[\cos(mkh\cos\theta) + \cos(mkh\sin\theta)] \approx r^{-2}[-1 + \cos(\omega\tau)]. \tag{31}$$

Using the Taylor series expansion for cosine functions, we have

$$a_0 + \sum_{m=1}^{M} a_m\left[2 + \sum_{j=1}^{\infty}(-1)^j \frac{m^{2j}(\cos^{2j}\theta + \sin^{2j}\theta)(kh)^{2j}}{(2j)!}\right] \approx \left[\sum_{j=1}^{\infty}(-1)^j \frac{r^{2j-2}(kh)^{2j}}{(2j)!}\right]. \tag{32}$$

Comparing coefficients of k^{2j}, we obtain

$$a_0 + 2\sum_{m=1}^{M} a_m = 0, \tag{33a}$$

$$\sum_{m=1}^{M} m^{2j}(\cos^{2j}\theta + \sin^{2j}\theta)a_m = r^{2j-2} \quad (j = 1, 2, \ldots, M). \tag{33b}$$

These equations indicate that the coefficient a_m is a function of θ. To obtain a single set of coefficients, we need to choose an optimal angle. Let

$$f(\theta) = (\cos\theta)^{2j} + (\sin\theta)^{2j}. \tag{34}$$

It is obvious that

$$f(\theta) = f(n\pi/2 \pm \theta), \quad f(\pi/8) = f(\pi/8 \pm n\pi/4). \tag{35}$$

If $\theta = \pi/8$ is used to solve Eq. (33b), the FD modeling can reach the highest $(2M)$th-order accuracy along eight directions: $\theta = (2n-1)\pi/8$ $(n = 1, 2, \ldots, 8)$. Therefore, we solve Eq. (33b) to obtain a_m by using $\theta = \pi/8$. Then, a_0 can be obtained by Eq. (33a).

3.3. 3D acoustic wave equation

The 3D acoustic wave equation is

$$\frac{\partial^2 p}{\partial x^2} + \frac{\partial^2 p}{\partial y^2} + \frac{\partial^2 p}{\partial z^2} = \frac{1}{v^2}\frac{\partial^2 p}{\partial t^2}. \tag{36}$$

When using the same FD for spatial derivatives, we have

$$\frac{\partial^2 p}{\partial x^2} \approx \frac{\delta^2 p}{\delta x^2} = \frac{1}{h^2}\left[a_0 p^0_{0,0,0} + \sum_{m=1}^{M} a_m\left(p^0_{-m,0,0} + p^0_{m,0,0}\right)\right], \tag{37a}$$

$$\frac{\partial^2 p}{\partial y^2} \approx \frac{\delta^2 p}{\delta y^2} = \frac{1}{h^2}\left[a_0 p^0_{0,0,0} + \sum_{m=1}^{M} a_m\left(p^0_{0,-m,0} + p^0_{0,m,0}\right)\right], \tag{37b}$$

$$\frac{\partial^2 p}{\partial z^2} \approx \frac{\delta^2 p}{\delta z^2} = \frac{1}{h^2}\left[a_0 p^0_{0,0,0} + \sum_{m=1}^{M} a_m\left(p^0_{0,0,-m} + p^0_{0,0,m}\right)\right], \tag{37c}$$

where

$$p^n_{m,l,j} = p(x + mh, y + lh, z + jh, t + n\tau). \tag{38}$$

The 2nd-order FD stencil for the time derivative is

$$\frac{\partial^2 p}{\partial t^2} \approx \frac{\delta^2 p}{\delta t^2} = \frac{1}{\tau^2}\left[-2p^0_{0,0,0} + \left(p^{-1}_{0,0,0} + p^1_{0,0,0}\right)\right]. \tag{39}$$

Using Eqs. (37a)–(37c) and (39), Eq. (36) is changed as follows:

$$\frac{1}{h^2}\left[3a_0 p^0_{0,0,0} + \sum_{m=1}^{M} a_m\left(p^0_{-m,0,0} + p^0_{m,0,0} + p^0_{0,-m,0} + p^0_{0,m,0} + p^0_{0,0,-m} + p^0_{0,0,m}\right)\right] \approx \frac{1}{v^2\tau^2}\left[-2p^0_{0,0,0} + \left(p^{-1}_{0,0,0} + p^1_{0,0,0}\right)\right]. \tag{40}$$

Let

$$p_{m,j}^{n} = e^{\mathrm{i}[k_x(x+mh)+k_y(y+lh)+k_z(z+jh)-\omega(t+n\tau)]}. \tag{41}$$

Take Eq. (41) into (40) and simplify it as follows:

$$3a_0 + \sum_{m=1}^{M} 2a_m[\cos(mk_xh) + \cos(mk_yh) + \cos(mk_zh)] \approx 2r^{-2}[-1 + \cos(\omega\tau)]. \tag{42}$$

Let

$$k_x = k\cos\theta\cos\phi, \quad k_y = k\cos\theta\sin\phi, \quad k_z = k\sin\theta, \tag{43}$$

where θ is the plane wave propagation angle measured from the horizontal plane perpendicular to z-axis, ϕ is the azimuth of the plane wave. Then Eq. (42) is written as

$$\frac{3}{2}a_0 + \sum_{m=1}^{M} a_m[\cos(mkh\cos\theta\cos\phi) + \cos(mkh\cos\theta\sin\phi) + \cos(mkh\sin\theta)] \approx r^{-2}[-1 + \cos(\omega\tau)]. \tag{44}$$

Using the Taylor series expansion for cosine functions, we have

$$\frac{3}{2}a_0 + \sum_{m=1}^{M} a_m\left[3 + \sum_{j=1}^{\infty}(-1)^j \frac{m^{2j}(\cos^{2j}\theta\cos^{2j}\phi + \cos^{2j}\theta\sin^{2j}\phi + \sin^{2j}\theta)(kh)^{2j}}{(2j)!}\right] \approx \left[\sum_{j=1}^{\infty}(-1)^j \frac{r^{2j-2}(kh)^{2j}}{(2j)!}\right]. \tag{45}$$

Comparing coefficients of k^{2j}, we obtain

$$a_0 + 2\sum_{m=1}^{M} a_m = 0, \tag{46a}$$

$$\sum_{m=1}^{M} m^{2j}(\cos^{2j}\theta\cos^{2j}\phi + \cos^{2j}\theta\sin^{2j}\phi + \sin^{2j}\theta)a_m = r^{2j-2} \quad (j = 1, 2, \ldots, M). \tag{46b}$$

These equations indicate that the coefficients a_m is a function of θ and ϕ. To obtain a single set of coefficients, we can choose an optimal angle. Let

$$f(\theta,\phi) = \cos^{2j}\theta(\cos^{2j}\phi + \sin^{2j}\phi) + \sin^{2j}\theta. \tag{47}$$

It is obvious that

$$f(\theta,\phi) = f(m\pi \pm \theta, n\pi/2 \pm \phi), \quad f(\pi/4, \pi/8) = f(\pi/4 \pm n\pi/2, \pi/8 \pm n\pi/4). \tag{48}$$

If $\theta = 0$ and $\phi = \pi/8$ are used to solve Eqs. (46b), the FD modeling can reach the highest $(2M)$th-order accuracy along 48 directions:
$\theta = (m-1)\pi,\ \phi = (2n-1)\pi/8\ (m = 1,2;\ n = 1,2,\ldots,8);\ \theta = (2m-1)\pi/8,\ \phi = (n-1)\pi/2\ (m = 1,2,\ldots,8;\ n = 1,2,3,4)$.
Therefore, we solve Eq. (46b) to obtain a_m by using $\theta = 0$ and $\phi = \pi/8$. Then, a_0 can be obtained by Eq. (46a).

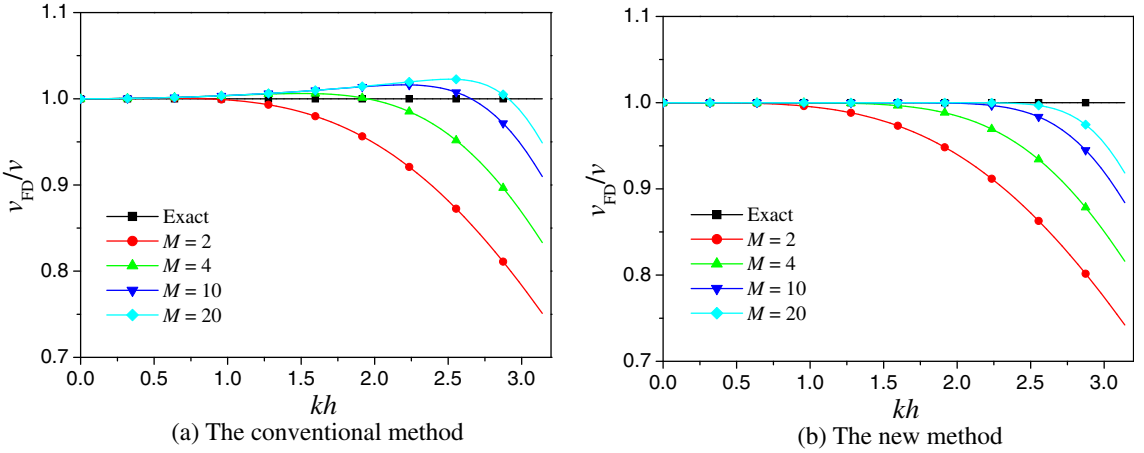

(a) The conventional method (b) The new method

Fig. 1. Plot of 1D dispersion curves of the conventional and the new methods for different space point numbers $2M + 1$, $M = 2$, 4, 10, 20, $v = 3000$ m/s, $\tau = 0.001$ s, $h = 10$ m.

4. Dispersion analysis

4.1. 1D dispersion analysis

We define a parameter δ to describe 1D dispersion of FD by using Eq. (15) as follows:

$$\delta = \frac{v_{FD}}{v} = \frac{2}{rkh}\sin^{-1}\sqrt{r^2\sum_{m=1}^{M} a_m \sin^2(mkh/2)}. \tag{49}$$

If δ equals 1, there is no dispersion. If δ is far from 1, a large dispersion will occur. Because kh is equal to π at the Nyquist frequency, kh only ranges from 0 to π when calculating δ.

Next, we compare the conventional and the new methods by the dispersion curves for different space point numbers, velocities and time steps.

Fig. 1 shows the variation of the dispersion parameter δ with kh for different space point numbers. The involved parameters are listed in the figure. This figure demonstrates that

- Dispersion decreases with the increase of M.
- For the conventional method, δ nearly equals 1 when $kh < 0.6$. The area where δ nearly equals 1 does not extend with the increase of M. That is, increase of M decreases the magnitude of the dispersion error without increasing the accuracy order.
- For the new method, the area where δ nearly equals 1 obviously extends with the increase of M.
- The accuracy of the new method is greater than that of the conventional method.

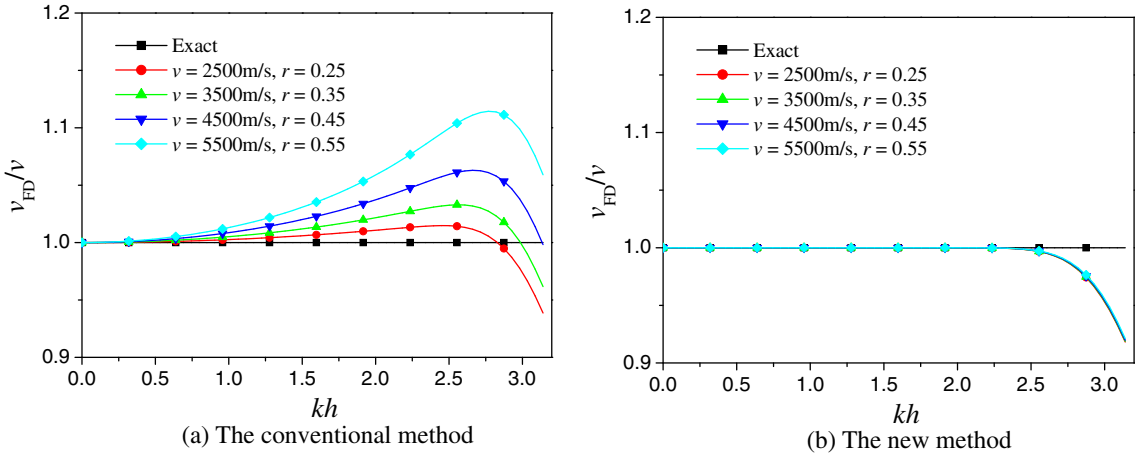

Fig. 2. Plot of 1D dispersion curves of the conventional and the new methods for different velocities, v = 2500, 3500, 4500 and 5500 m/s, that is, r = 0.25, 0.35, 0.45 and 0.55, τ = 0.001 s, h = 10 m, M = 20.

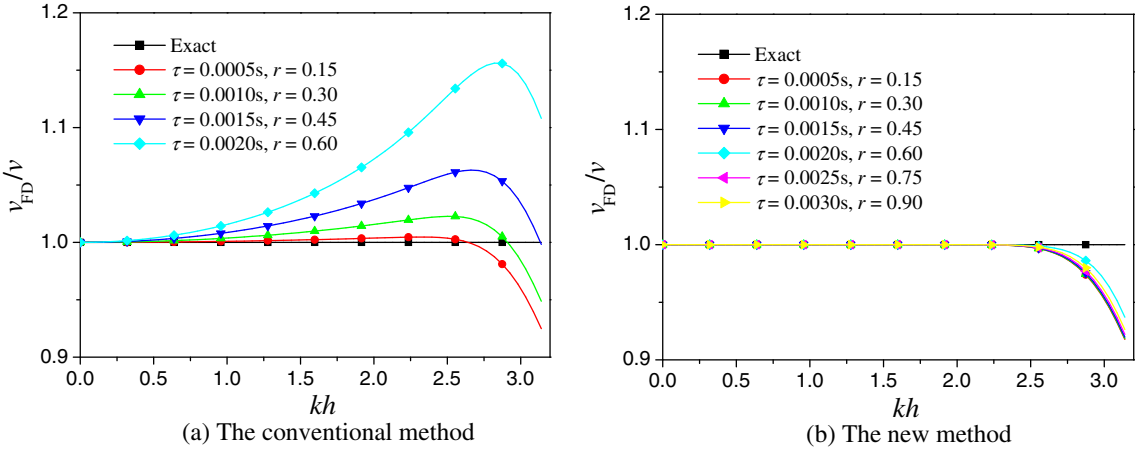

Fig. 3. Plot of 1D dispersion curves of the conventional and the new methods for different time steps, τ = 0.0005, 0.0010, 0.0015 and 0.0020 s, that is, r = 0.15, 0.30, 0.45 and 0.60. And τ = 0.0025 and 0.0030 s, that is, r = 0.75 and 0.70, are added for the new method. v = 3000 m/s, h = 10 m, M = 20.

Fig. 2 shows the variation of the dispersion parameter δ with kh for different velocities. The involved parameters are listed in the figure also. From this figure, we can see that the dispersion curves change greatly with the variation of velocity for the conventional method, while they change slightly for the new method. The dispersion characteristics of the new method, mainly dependent on M, are more stable than the conventional method.

Fig. 3 illustrates the effect of time step on dispersion. For the conventional method, the dispersion becomes stronger with the increase of time step. Moreover, a lager time step, such as 0.0025 s, 0.0030 s in this example, makes the recursion

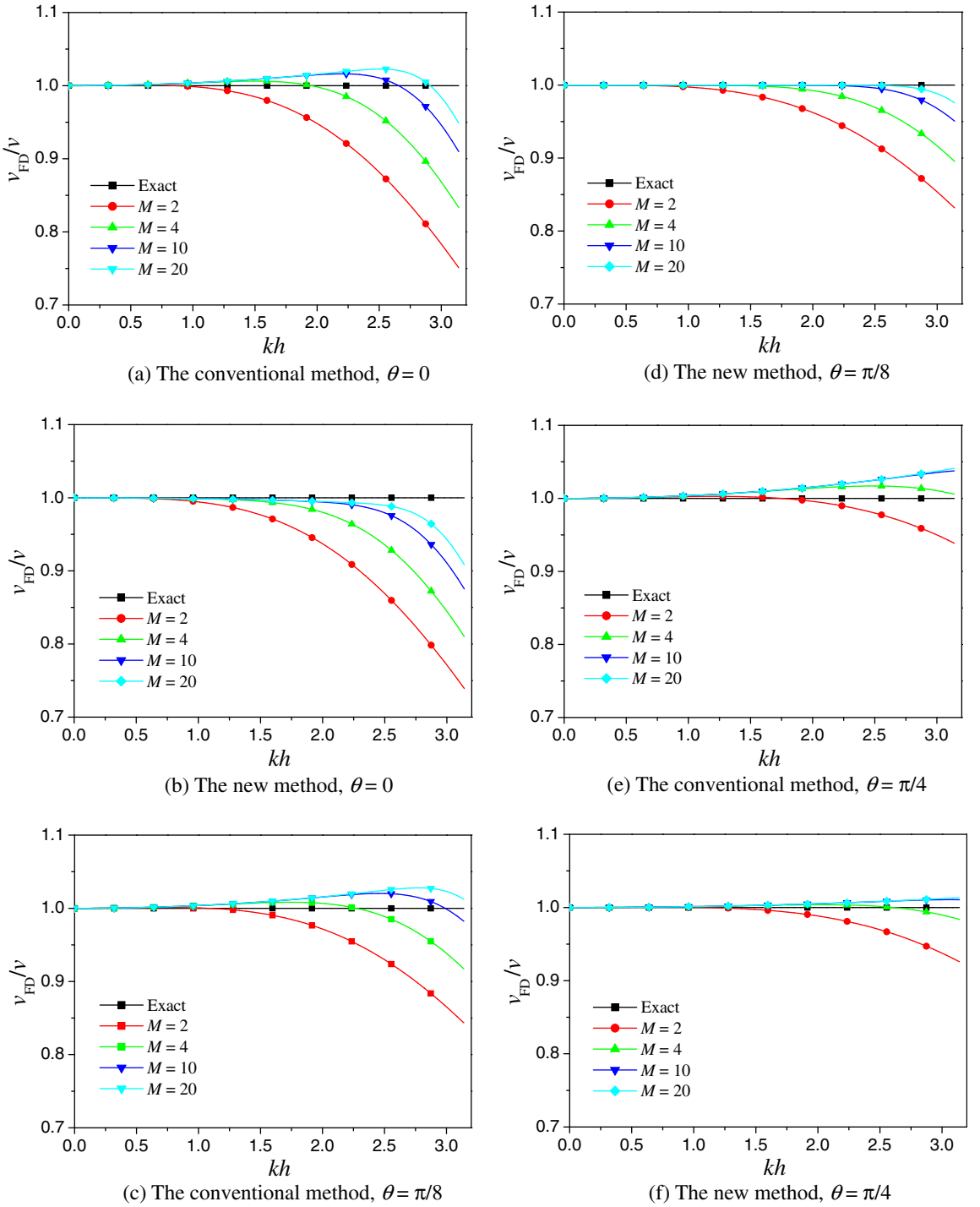

(a) The conventional method, $\theta = 0$

(d) The new method, $\theta = \pi/8$

(b) The new method, $\theta = 0$

(e) The conventional method, $\theta = \pi/4$

(c) The conventional method, $\theta = \pi/8$

(f) The new method, $\theta = \pi/4$

Fig. 4. Plot of 2D dispersion curves of the conventional and the new methods for different propagation angles, $\theta = 0$, $\pi/4$, $\pi/8$, and different space point numbers $2M + 1$, $M = 2$, 4, 10 and 20. $v = 3000$ m/s, $\tau = 0.001$ s, $h = 10$ m.

unstable. However, the new method is always stable and its dispersion decreases with the increase of time step. Therefore, the new method can adopt a larger time step and reach greater accuracy.

4.2. 2D dispersion analysis

2D dispersion $\delta(\theta)$ is defined as follows by using Eq. (31)

$$\delta = \frac{v_{FD}}{v} = \frac{2}{rkh}\sin^{-1}\sqrt{r^2\sum_{m=1}^{M} a_m(\sin^2(mkh\sin\theta/2) + \sin^2(mkh\cos\theta/2))}. \tag{50}$$

Since $\delta(\theta) = \delta(\theta + \pi/2), \delta(\theta)$ is a periodic function with a period of $\pi/2$. Considering $\delta(\theta) = \delta(\pi/2 - \theta)$, we only calculate $\delta(\theta)$ with the variation of θ from 0 to $\pi/4$.

Fig. 4 shows the 2D dispersion curves of the conventional and new methods along three directions for different space point numbers. From the figure, we can see that

- With the increase of wavenumber, the dispersion generally increases and the accuracy decreases.
- With the increase of the space point number, the dispersion generally decreases and the accuracy increases. However, the area where δ nearly equals 1 does not extend with the increase of M for the conventional method. This area does extend for the new method.
- The dispersion of the new method is generally smaller than that of the conventional method.

Fig. 5 shows the 2D dispersion curves of the conventional and the new method along five directions when $M = 10$, which also demonstrates that the accuracy of the new method is greater than that of the conventional method.

4.3. 3D dispersion analysis

3D dispersion $\delta(\theta, \phi)$ is defined as follows by using Eq. (44)

$$\delta = \frac{v_{FD}}{v} = \frac{2}{rkh}\sin^{-1}\sqrt{r^2\sum_{m=1}^{M} a_m(\sin^2(mkh\sin\theta/2) + \sin^2(mkh\cos\theta\sin\phi/2) + \sin^2(mkh\cos\theta\cos\phi/2))}. \tag{51}$$

5. Stability analysis

5.1. 1D stability condition

The 1D recursion equation of FD can be obtained from Eq. (5) as follows:

$$p_0^1 = (r^2a_0 + 2)p_0^0 + r^2\sum_{m=1}^{M} a_m(p_{-m}^0 + p_m^0) - p_0^{-1}. \tag{52}$$

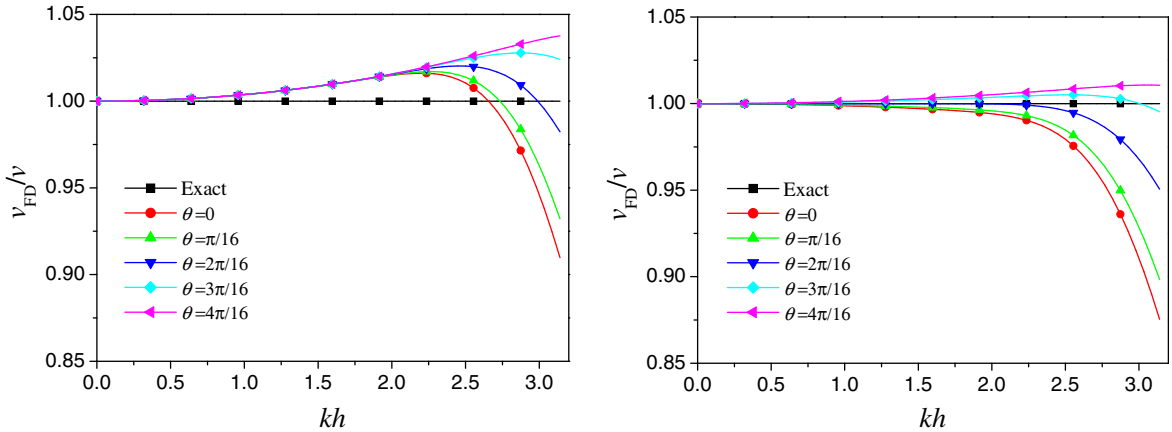

(a) The conventional method (b) The new method

Fig. 5. Plot of 2D of dispersion curves of the conventional and the new methods. The propagation angles are 0, $\pi/16$, $2\pi/16$, $3\pi/16$ and $4\pi/16$. $v = 3000$ m/s, $\tau = 0.001$ s, $h = 10$ m, $M = 10$.

Using the conventional eigenvalue method of stability analysis, we let

$$q_m^0 = p_m^{-1}, \quad \boldsymbol{U}_m^0 = (p_m^0, q_m^0)^T = \boldsymbol{W}^0 e^{ikmh}, \boldsymbol{U}_m^1 = (p_m^1, q_m^1)^T = \boldsymbol{W}^1 e^{ikmh}. \tag{53}$$

According to Eqs. (52) and (53), we obtain

$$\boldsymbol{W}^1 = \boldsymbol{G}\boldsymbol{W}^0 = \begin{bmatrix} g & -1 \\ 1 & 0 \end{bmatrix} \boldsymbol{W}^0, \tag{54}$$

where $\boldsymbol{G}$ is a transition matrix,

$$g = 2 + 2r^2 \sum_{m=1}^{M} a_m [\cos(mkh) - 1]. \tag{55}$$

When the absolute values of the transition matrix eigenvalues are less than or equal to 1, the recursion is stable. If $|g| \leqslant 2$, the roots of the eigenvalue equation $\lambda^2 - g\lambda + 1 = 0$ will be less than or equal to 1.

Since the error generally increases with the increase of the wavenumber, we consider the maximum wavenumber – the Nyquist wavenumber, that is

$$k = \pi/h. \tag{56}$$

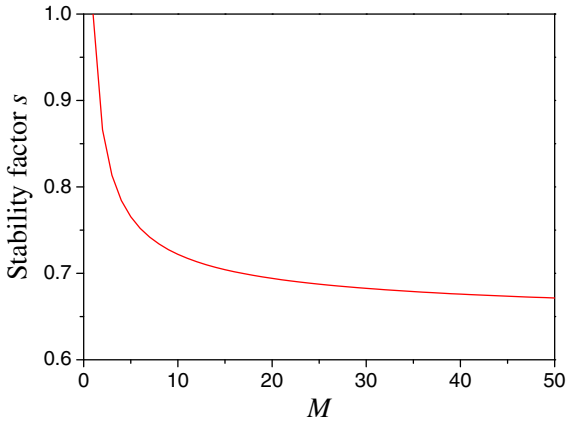

(a) The variation of stability factor s with M for the conventional method

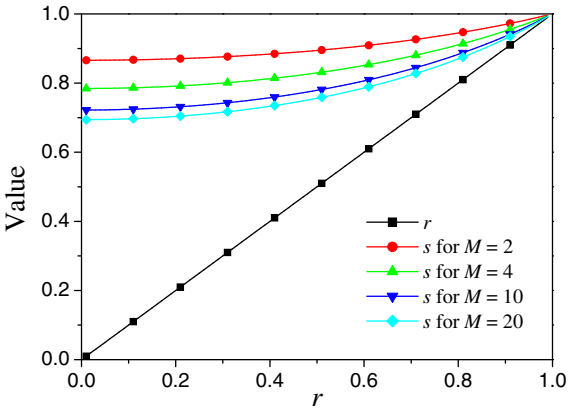

(b) The variation of stability factor s with M and r for the new method.

Fig. 6. Plot of 1D stability conditions for the conventional and the new methods. The method is stable when $r \leqslant s$.

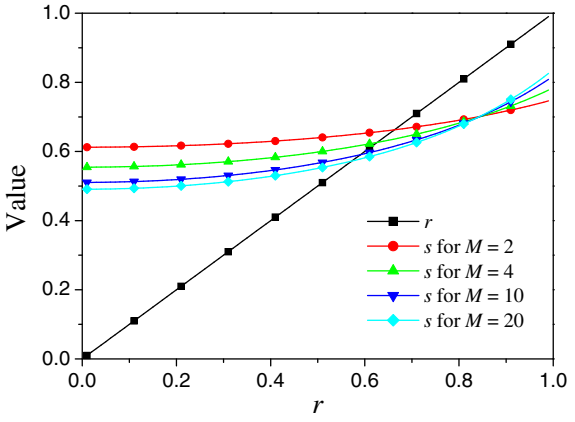

(a) The variation of stability factor s with M and r for the new method.

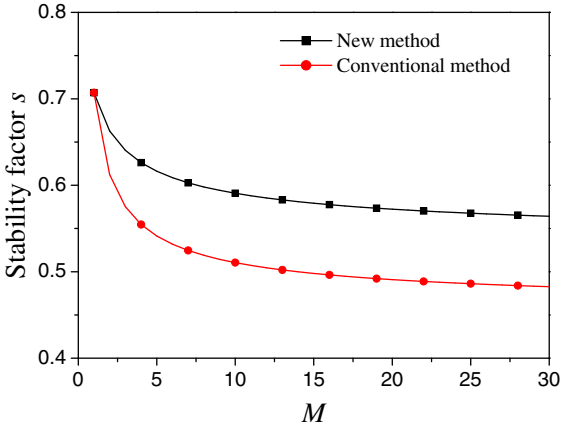

(b) Stability condition of the conventional and the new methods. Stability factor of the new method shown here is the maximum value of s satisfying Eq. (52) $r \leq s$.

Fig. 7. Plot of 2D stability conditions for the conventional and the new methods. The method is stable when $r \leqslant s$.

Substituting Eq. (56) into (55), we have

$$g = 2 - 4r^2 \sum_{m=1}^{M_1} a_{2m-1}, \tag{57}$$

where $M_1 = \text{int}[(M+1)/2]$, int is a function to get the integer part of a value.

Therefore, the 1D stability condition is

$$\left| 2 - 4r^2 \sum_{m=1}^{M_1} a_{2m-1} \right| \leqslant 2, \tag{58}$$

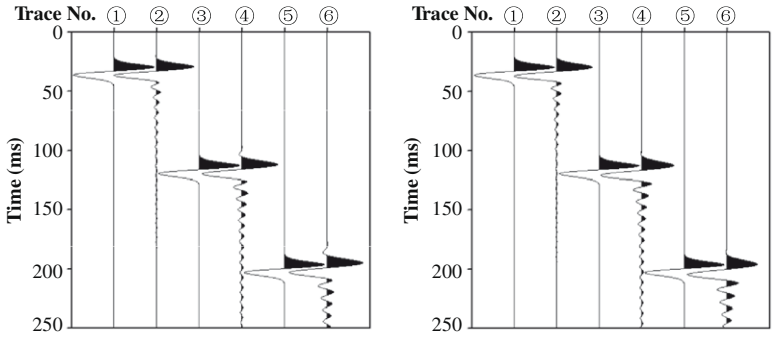

(a) The conventional (left) and the new (right) methods, $M = 4$

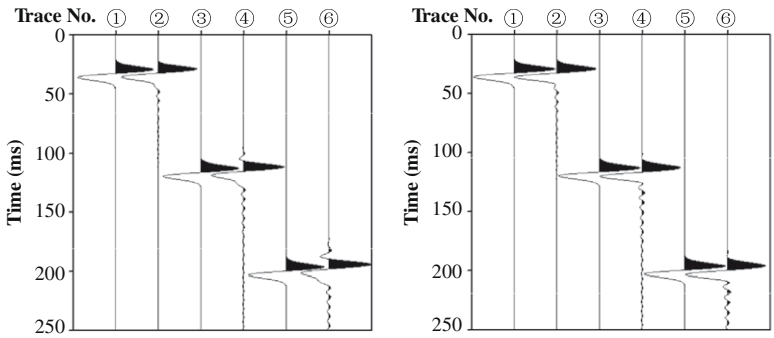

(b) The conventional (left) and the new (right) methods, $M = 10$

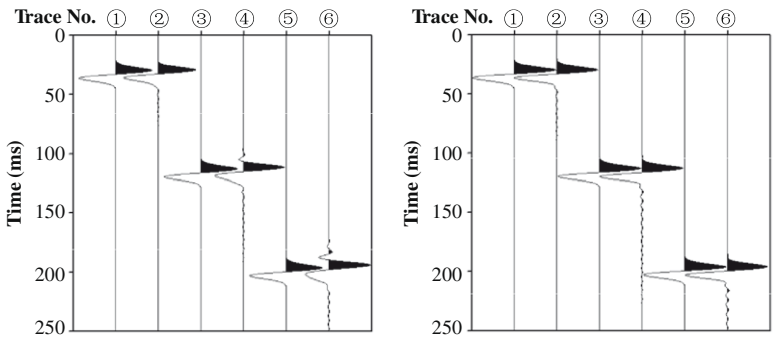

(c) The conventional (left) and the new (right) methods, $M = 20$

Fig. 8. 1D modeling records computed by the conventional and the new methods for different space point numbers. ①, ③ and ⑤ are analytic solutions; ②, ④ and ⑥ are modeling results. Distances between source center and these three receivers are 100, 350 and 600 m, respectively. $\alpha^2 = 2$, $v = 3000$ m/s, $h = 10$ m, $\tau = 0.001$ s.

that is,

$$r \leqslant \left(\sum_{m=1}^{M_1} a_{2m-1} \right)^{-1/2}. \tag{59}$$

where $a_{2m-1} > 0$, which can be obtained from Eq. (20) for $r < 1$.

5.2. 2D and 3D stability conditions

Similarly, stability conditions for 2D, 3D acoustic wave equation modeling can be derived as follows, respectively

$$r \leqslant \left(2 \sum_{m=1}^{M_1} a_{2m-1} \right)^{-1/2}, \tag{60}$$

$$r \leqslant \left(3 \sum_{m=1}^{M_1} a_{2m-1} \right)^{-1/2}. \tag{61}$$

5.3. 1D stability calculation and analysis

To calculate and analyze the stability of the FD, we define 1D stability factor s as follows according to Eq. (59)

$$s = \left(\sum_{m=1}^{M_1} a_{2m-1} \right)^{-1/2}. \tag{62}$$

For the conventional method, the FD coefficients depend only on M. We calculate the variation of s with M, which is shown in Fig. 6(a). From the figure, we can see that the area of r for stable recursion decreases with the increase of M.

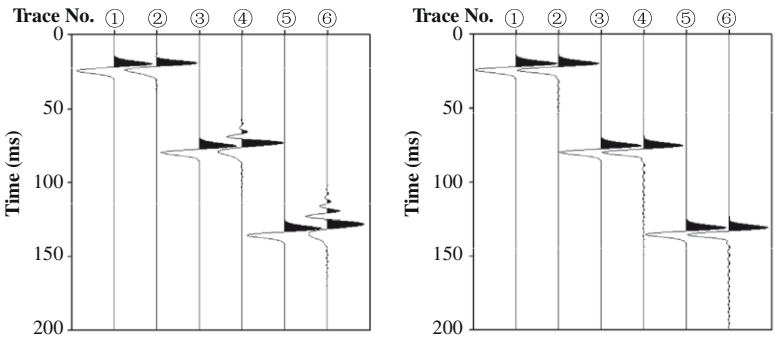

(a) The conventional (left) and the new (right) methods, v = 4500m/s

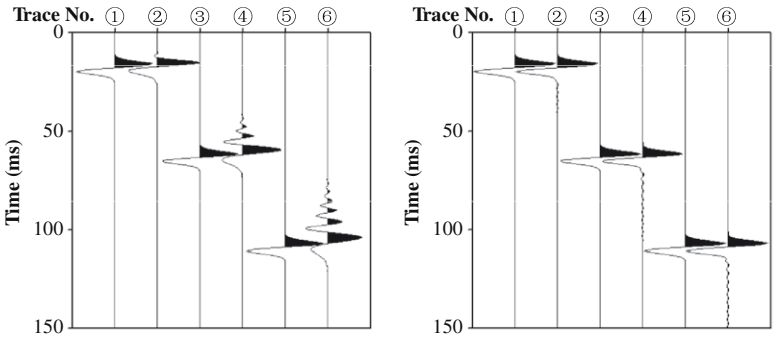

(b) The conventional (left) and the new (right) methods, v = 5500m/s

Fig. 9. 1D modeling records computed by the conventional and the new methods for different velocities. ①, ③ and ⑤ are analytic solutions; ②, ④ and ⑥ are modeling results. Distances between source center and these three receivers are 100, 350 and 600 m, respectively. $\alpha^2 = 2$, $h = 10$ m, $\tau = 0.001$ s, $M = 20$.

For the new method, the FD coefficients depend on both M and r. We calculate the variation of s with M and r, shown in Fig. 6(b), where r ranges from 0.01 to 0.99 and $M = 2, 4, 10, 20$. The figure demonstrates that $r \leqslant s$. Therefore, the new method is always stable when $r \leqslant 1$ since the FD coefficients are designed for the given M and r.

5.4. 2D stability calculation and analysis

The 2D stability factor s is defined as follows according to Eq. (60)

$$s = \left(2\sum_{m=1}^{M_1} a_{2m-1}\right)^{-1/2}. \tag{63}$$

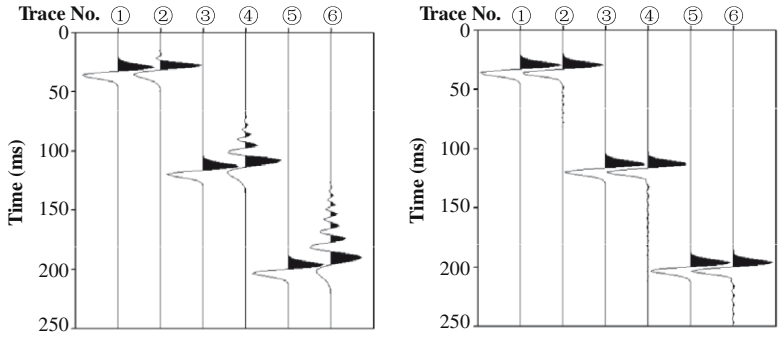

(a) The conventional (left) and the new (right) methods, $\tau = 0.002$s

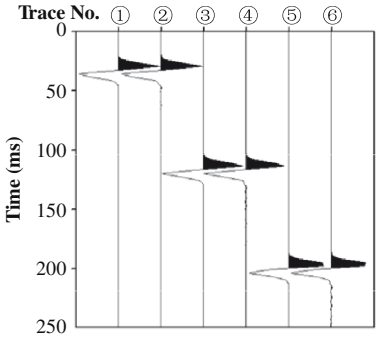

(b) The new method, $\tau = 0.003$s

Fig. 10. 1D modeling records computed by the conventional and new methods for different time steps. ①, ③ and ⑤ are analytic solutions; ②, ④ and ⑥ are modeling results. Distances between source center and these three receivers are 100, 350 and 600 m, respectively. $\alpha^2 = 2$, $v = 3000$ m/s, $h = 10$ m, $M = 20$. The conventional is unstable when $\tau = 0.003$.

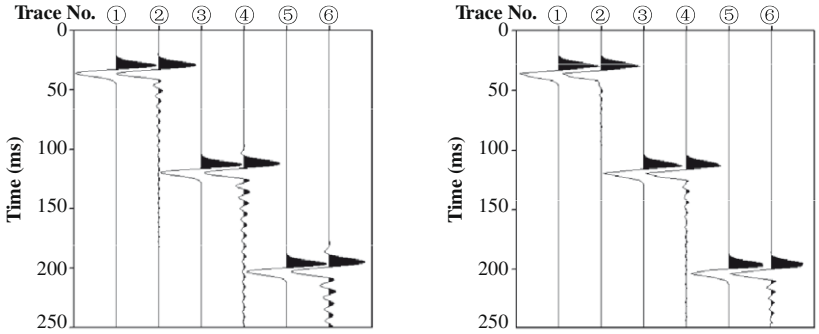

(a) The conventional method, $\tau = 0.001$s (b) The new method, $\tau = 0.003$s

Fig. 11. 1D modeling records computed by the conventional and the new methods for different time steps with the low-order accuracy. ①, ③ and ⑤ are analytic solutions; ②, ④ and ⑥ are modeling results. Distances between source center and these three receivers are 100, 350 and 600 m, respectively. $\alpha^2 = 2$, $v = 3000$ m/s, $h = 10$ m, $M = 4$.

Fig. 7(a) shows the variation of stability factor s with M and r for the new method. When r is large, the new method is unstable. We calculate the maximum value of s satisfying Eq. (60), which is shown with the conventional method in Fig. 7(b). The figure demonstrates that the new method can adopt a larger r than the conventional method when $M > 1$.

6. Modeling examples

6.1. 1D modeling

In all the 1D numerical modeling examples shown in this paper, the following initial conditions are used

$$p(x,t)|_{t=0} = (x - x_0)e^{-\frac{\alpha^2}{4h^2}(x-x_0)^2}, \tag{64a}$$

$$\left.\frac{\partial p(x,t)}{\partial t}\right|_{t=0} = 0, \tag{64b}$$

where x_0 is the location of the source center, and α^2 is an attenuation coefficient.

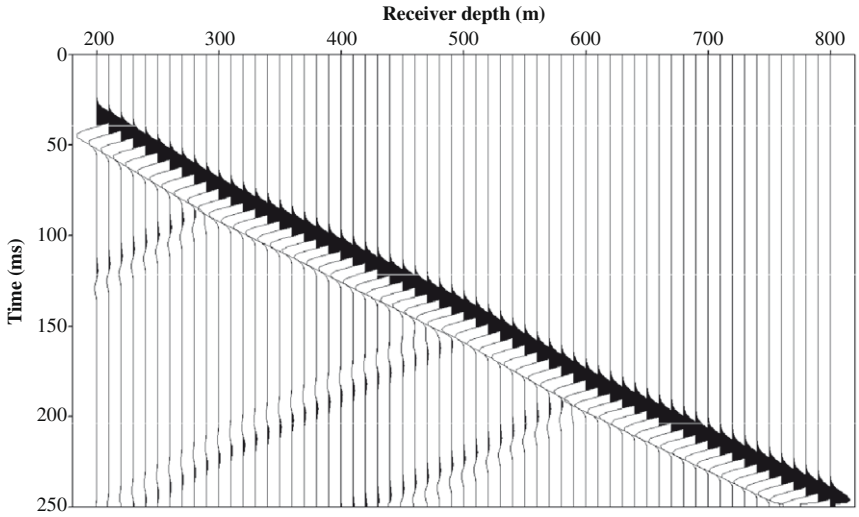

(a) The nearly analytic solution

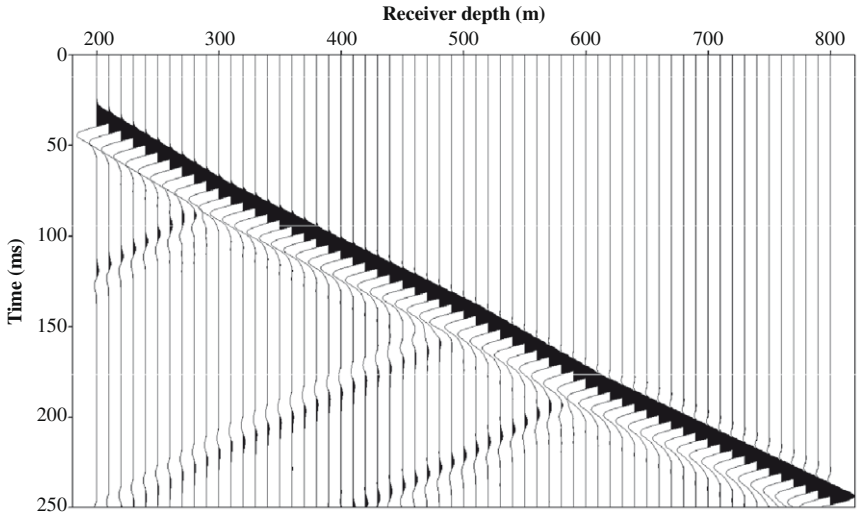

(b) The conventional method, $\tau = 0.001$s

Fig. 12. 1D modeling records for an inhomogeneous model computed by the conventional and the new methods. The model has four layers, whose velocities are 2500, 3000, 2600 and 3100 m/s, respectively, from shallow to deep. The depths of three interfaces are 305, 505 and 605 m, respectively; source depth is 100 m, $\alpha^2 = 1.5$. (a) The nearly analytic solution, calculated by the 2nd-order FD method with a very small grid size and time step, that is, $h = 2$ m, $\tau = 0.00025$ s, $M = 1$. For (b), (c) and (d), $h = 10$ m, $M = 10$.

Both the conventional and the new FD methods are used to simulate acoustic wave propagation in 1D homogeneous media. v is 3000 m/s, the grid size h is 10 m. Fig. 8 shows the seismic records computed by the conventional and the new methods for different space point numbers. The figure demonstrates that the accuracy increases with the increase of space point number. Compared with the analytic solutions, the modeling results from the new method show less dispersion than the conventional method, and the waveforms retain their shapes better than the conventional method. Fig. 9 shows the modeling records for different velocities. The variation of the velocity affects the results of the conventional method more than the new method because the FD coefficients of the new method depend on velocity. Fig. 10 shows the modeling records by the conventional and the new methods for different time steps. The records computed by the conventional method in Figs. 8(c) and 10(a) show that the dispersion increases with increasing time step. However, comparing Figs. 8(c), 10(a) and (b), we find that the dispersion of the new method decreases with the increasing time step. Since the conventional method is unstable and the new method is stable and more accurate when $\tau = 0.003$, the new method can adopt a larger time step in the modeling given by the same discretization. Fig. 11 shows the records with the low-order accuracy, which also demonstrates that the new method can use a larger time step and obtain a better result at the same time.

Next, we use the conventional and the new methods to perform numerical modeling for an inhomogeneous model. The involved parameters are listed in the figure; the records obtained by the numerical modeling are shown in

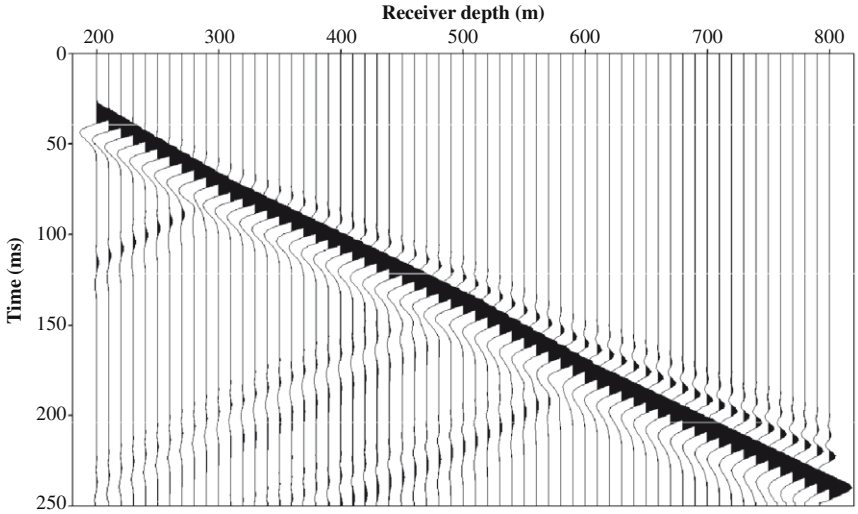

(c) The conventional method, $\tau = 0.002$s

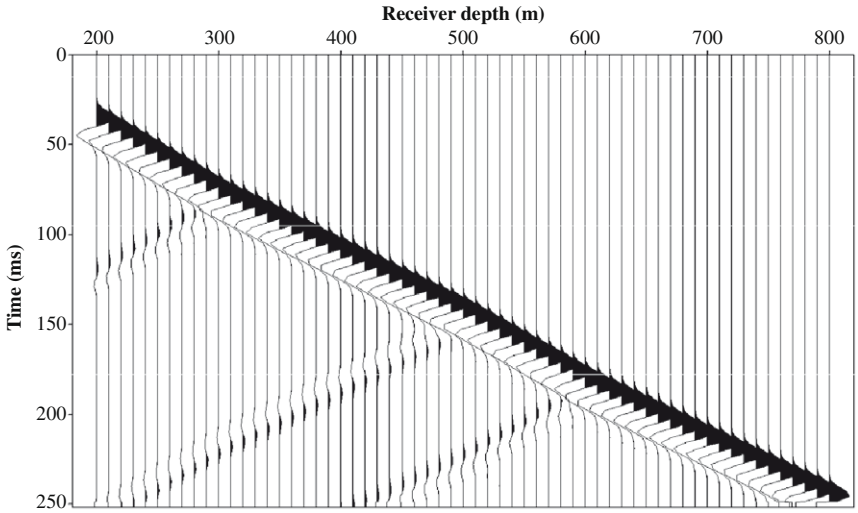

(d) The new method, $\tau = 0.003$s

Fig. 12 (*continued*)

Fig. 12. Down-going (i.e., transmission) and up-going (i.e., reflection) waves can be clearly seen in this figure. Fig. 12(a) is the nearly analytic solution, calculated by the 2nd-order FD method with a very small grid size (i.e., 2 m) and time step (i.e., 0.00025 s). Note that for the 2nd-order FD, the new method and the conventional method are the same. Fig. 12(b) and (c) are calculated by the conventional method for different time steps (i.e., 0.001 and 0.002 s). The record has lower dispersion for the smaller time step, which coincides with Fig. 3(a). Variations of transmission waveform can be clearly seen in Fig. 12(b) even for the smaller time step. Fig. 12(c) shows large dispersion because the waveform in the record changes significantly with the increase of receiver depth. The reason is that the conventional method is of 2nd-order accuracy (see Fig. 1(a)) and thus accurate modeling results can be obtained only by using a very small grid size and time

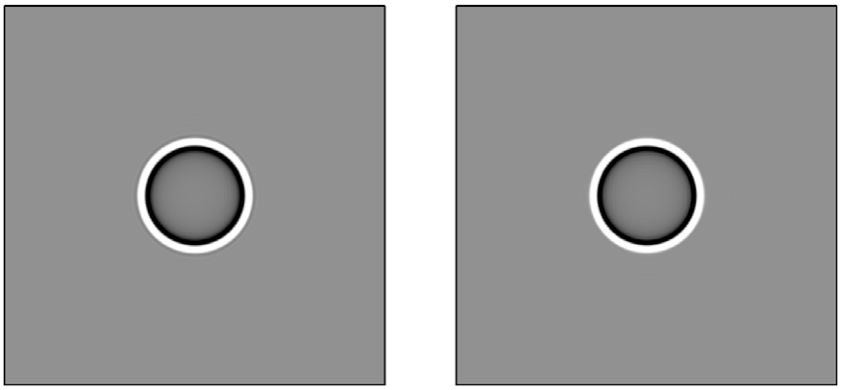

(a) Snapshots at 0.1s by the conventional (left) and the new (right) methods

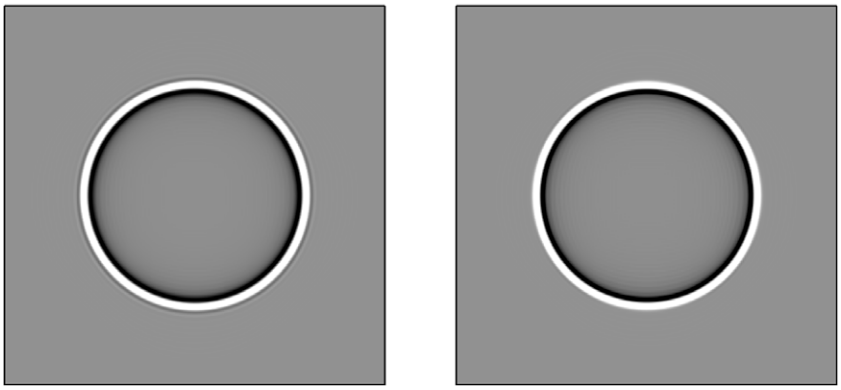

(b) Snapshots at 0.2s by the conventional (left) and the new (right) methods

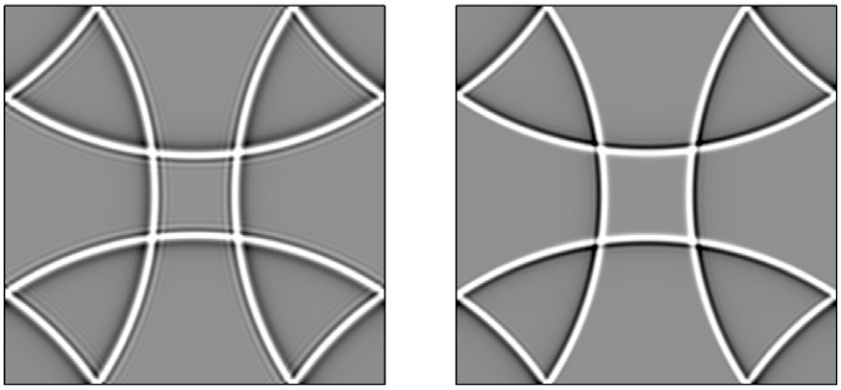

(c) Snapshots at 0.6s by the conventional (left) and the new (right) methods

Fig. 13. 2D modeling snapshots and records for a homogeneous model computed by the conventional and the new methods. $v = 3000$ m/s. The model size is 2000 m $\times$ 2000 m. $\tau = 0.001$ s, $h = 10$ m, $M = 10$. The source is located in the model center. A one-period sine function with 50 Hz frequency is used to generate vibration. No absorbing boundary conditions are used in the modeling.

step, or very low frequencies, or very low velocities. However, the accuracy order of the new method increases with the increase of the length of FD stencil (see Fig. 1(b)), the dispersion of the new method depends mainly on the length of spatial FD stencils and little on velocities and time steps (see Figs. 2(b) and 3(b)), which means that a larger time step can be used in the modeling as long as the Courant number is not greater than 1 to maintain the modeling accuracy and decrease the calculation amount. Fig. 12(d) displays the modeling records by the new method with a larger time step (i.e., 0.003 s). The records retain the waveform very well for different receiver depths and very close to the nearly analytic solution of Fig. 12(a), showing that the new method has greater accuracy, and higher efficiency that the conventional method.

6.2. 2D modeling

In this section, we show results from numerical modeling by the conventional and the new methods using a 2D homogeneous model and an inhomogeneous model under the same discretization.

Fig. 13 shows the modeling snapshots and records for the homogeneous model. The waveform corresponding to the new method retains its shape better than that by the conventional method, which demonstrates that the new method has greater accuracy and smaller dispersion. Fig. 14 shows the modeling snapshots and records for a so-called 2D Society of Exploration Geophysicists/European Association of Geoscientists and Engineers (SEG/EAGE) salt model. Here, we simply extended the model spatially to avoid reflections from the top and other edges of the model. Variations of waveform resulting from grid dispersion effects can be seen in Fig. 14(b) and (f) by the conventional method. However, Fig. 14(c) and (g) show that the new method maintains the waveform better and thus has smaller dispersion. The modeling results demonstrate that the new 2D method has greater accuracy and smaller dispersion than the conventional method.

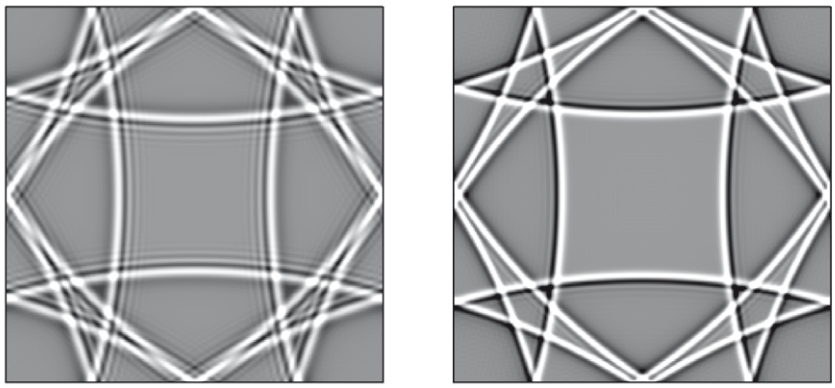

(d) Snapshots at 1.2s by the conventional (left) and the new (right) methods

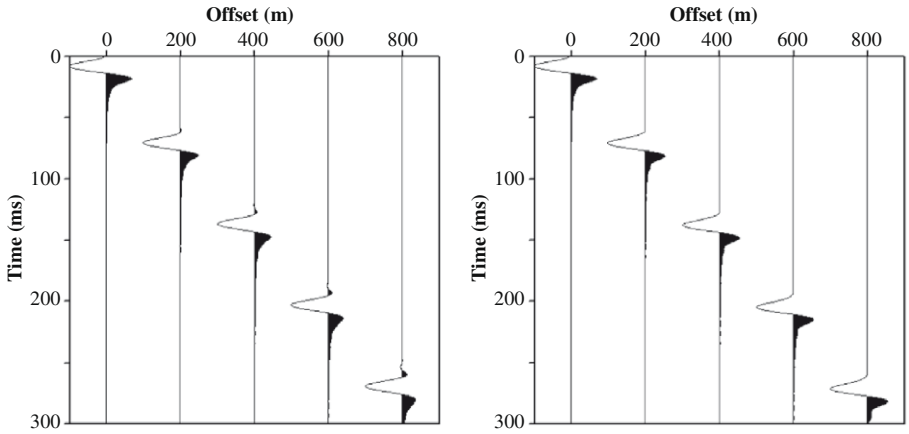

(e) Records from 5 receivers by the conventional (left) and the new (right) methods.

Fig. 13 (*continued*)

7. Discussion

We discuss three issues. The first is the influence of FD stencil length on numerical modeling for inhomogeneous media. The second is the choice of optimal FD stencil length to balance the modeling accuracy and efficiency. The third is an extension of our method to high-order staggered-grid FD for the acoustic wave equation where the density is inside a partial derivative. As examples for these three issues, we only discuss the 1D case.

7.1. Influence of FD stencil length

We use numerical modeling tests to investigate the influence of FD stencil length on the acoustic wave equation modeling for a 1D inhomogeneous model. The model has 10 layers, whose thicknesses vary from 20 to 50 m and velocities vary from 2500 to 5000 m/s. An analytic solution is obtained by the 2nd-order FD modeling with a very small grid size (2 m) and time step (0.00025 s). Different lengths of FD stencils are used to perform numerical modeling by the new method with a large grid size (10 m) and time step (0.002 s). The detailed parameters for the model and modeling are shown in the caption of Fig. 15. A lower frequency source is adopted in Fig. 15(a) and a higher frequency source is used in Fig. 15(b). From the figure, it follows that

- The records change little for different FD stencil lengths when the source frequency is lower and they are almost identical to the nearly analytic solution.
- The records vary substantially with FD stencil length for the higher frequency source. With the increase of the FD stencil length, the modeling accuracy increases and the record gradually approaches the nearly analytic solution.

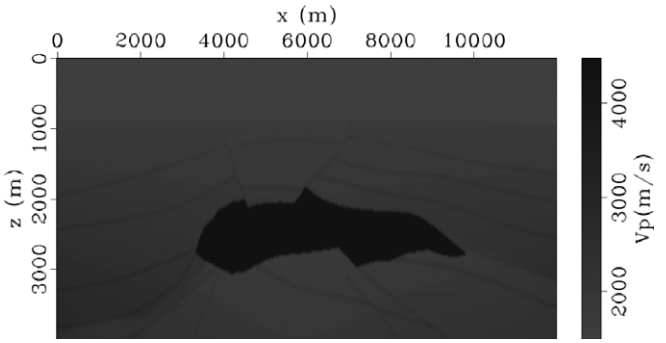

(a) The SEG/EAGE salt model

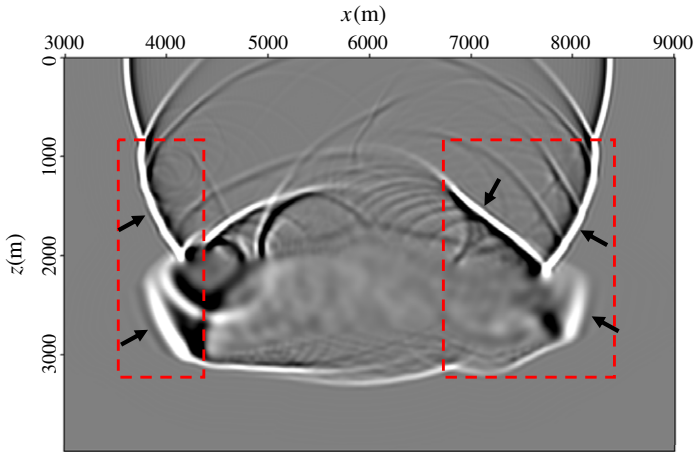

(b) Snapshot at t=1.6s by the conventional method

Fig. 14. 2D modeling snapshots and records for the SEG/EAGE salt model, respectively, computed by the conventional and the new methods. $\tau = 0.002$ s, $h = 20$ m, $M = 20$. The source is located at (6000 m, 20 m). A one-period sine function with 20 Hz frequency is used to generate vibration. The depth of receivers is 20 m.

We can conclude that even when the length of FD stencil is significantly larger than the thicknesses of layers, the results are quite satisfactory. The reason is that the model is discretized accurately here. In practice, it is difficult to discretize a model using very fine grids everywhere since the number of grid points becomes very large which leads to large memory and enormous computation time.

7.2. Optimal FD stencil length

It is known that the accuracy and the calculation amount of FD modeling are directly proportional to the FD stencil length and are inversely proportional to the grid size and the time step. When the FD stencil length is increased, the accuracy and the calculation amount of modeling are also increased. To maintain the modeling accuracy, the grid size and the time step can be increased at the same time. Therefore, for a given accuracy of modeling, there is a tradeoff between the accuracy and the calculation amount, which depends on the FD stencil length, the grid size and the time step. We can possibly find an optimal FD stencil length that provides the minimum calculation amount.

For 1D acoustic wave equation modeling, the total number of multiplication operations is N_M and the total number of addition or subtraction operations is N_A given by (Appendix A)

$$N_M = \frac{4\pi^2 f_{max}^2 LT}{v_{min} r_{max}} \frac{(M+1)}{\beta_{max}^2}, \quad N_A = 2N_M, \tag{65}$$

where L and T are the spatial length and the temporal length of the modeling, respectively, v_{min} is the minimum velocity, f_{max} is the maximum frequency of the wavefield, r_{max} is the maximum Courant number and $r_{max} \leqslant 1$, $\beta = kh$, β_{max} is determined

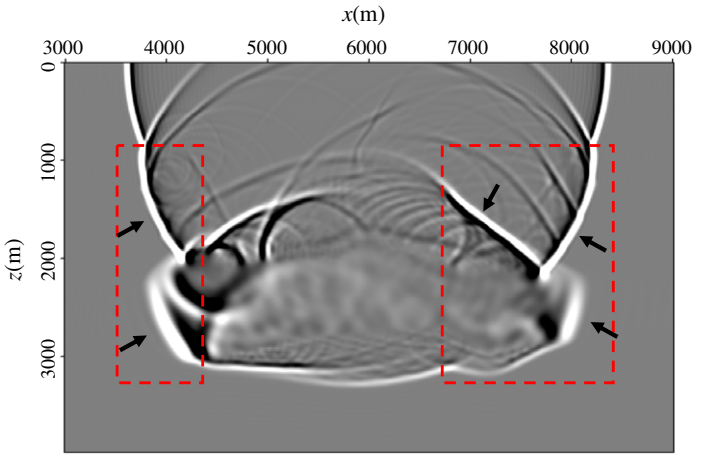

(c) Snapshots at t=1.6s by the new method

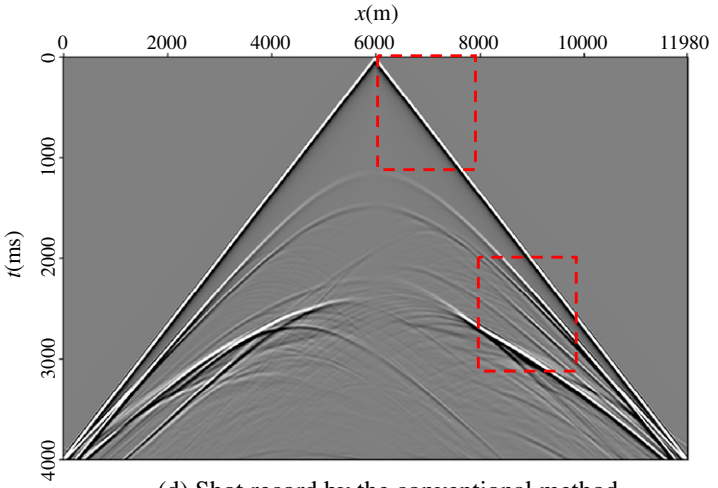

(d) Shot record by the conventional method

Fig. 14 (*continued*)

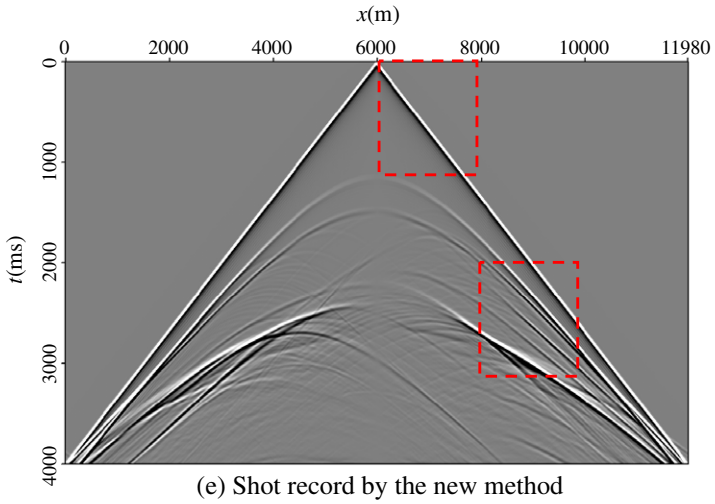

(e) Shot record by the new method

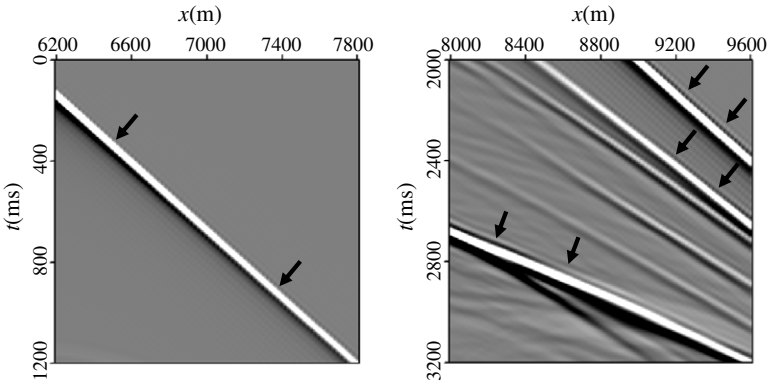

(f) Zoom of (d)

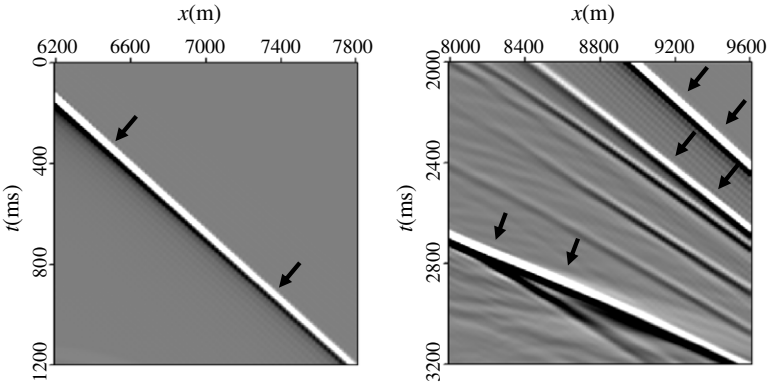

(g) Zoom of (e)

Fig. 14 (*continued*)

by Eq. (68) for a given positive number η and a given integer number M. For a given task of numerical modeling, L, T, $v_{\min}$ and $f_{\max}$ are known. When $r_{\max}$ and η are given, the calculation amount is directly proportional to $(M+1)\beta_{\max}^{-2}$.

Fig. 16(a) shows the variations of $\beta_{\max}$ and $(M+1)\beta_{\max}^{-2}$ with M for different values of η, it can be seen that

- $\beta_{\max}$ increases with the increase of M and η.
- There is a minimum in the function of $(M+1)\beta_{\max}^{-2}$. The optimal length of FD stencil can be determined from the minimum.

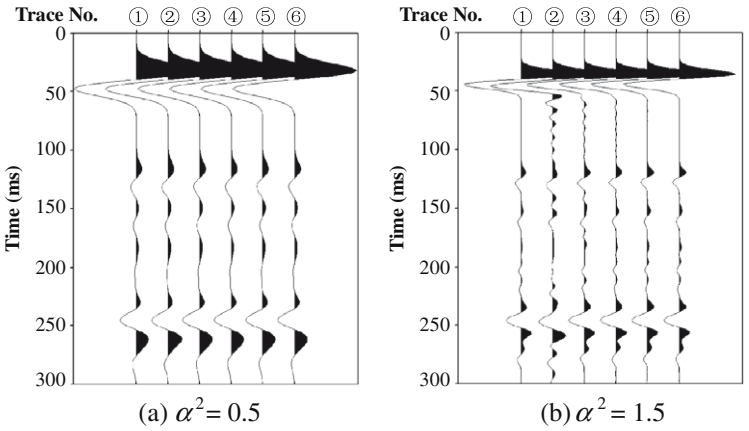

Fig. 15. 1D modeling records computed by the new FD method with different FD stencil lengths for an inhomogeneous model. The model has 10 layers, whose velocities are 2500, 3000, 3300, 3500, 3800, 4000, 5000, 3500, 4000 and 4500 m/s, respectively, from shallow to deep. Nine interfaces' depths are 1205,1255, 1305, 1325, 1355, 1405, 1435, 1475 and 1405 m, source depth is 100 m, receiver depth is 200 m. ① is nearly analytic solution, calculated by the 2nd-order FD method with a very small grid size and time step, that is, $h = 2$ m, $\tau = 0.00025$ s, $M = 1$. ②, ③, ④, ⑤ and ⑥ are calculated by the new FD method with different values of M, they are 2, 5, 10, 20 and 50, respectively, $h = 10$ m, $\tau = 0.002$ s.

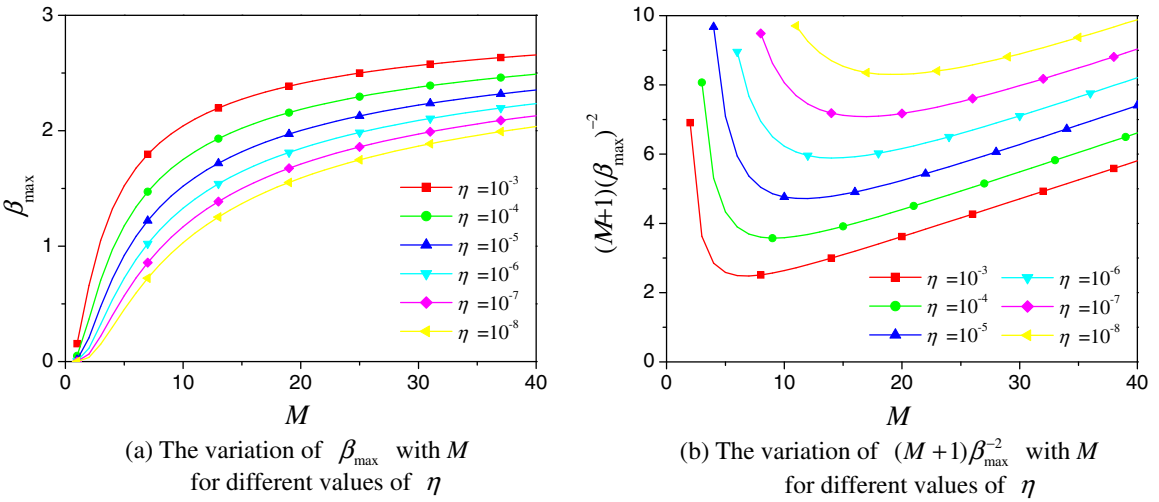

Fig. 16. Plot of the variations of β_{max} and $(M+1)\beta_{max}^{-2}$ with M for different values of η. The calculation amount for 1D acoustic wave equation modeling is directly proportional to $(M+1)\beta_{max}^{-2}$. β_{max} is obtained by scanning the Courant number r. r ranges from the minimum Courant number r_{min} to the maximum Courant number r_{max} with an increment Δr. We find that β_{max} is mainly dependent on r_{min}, and β_{max} is nearly constant when r_{min} is not very close to zero. Note that r_{max} can be set to 1. If minimum velocity is greater than one tenth of maximum velocity, $r_{min} > 0.1$. Here, $r_{min} = 0.1$, $r_{max} = 1$, $\Delta r = 0.01$ and Eq. (68) are used to calculate β_{max}.

7.3. Time–space domain high-order staggered-grid FD method

To show how the proposed scheme can be extended to acoustic wave equation with variable densities, we develop a new time–space domain high-order staggered-grid FD method. The details are given in Appendix B. The 1D wave equation, staggered-grid FD coefficients, accuracy, dispersion and stability condition are given in Eqs. (75), (86) and (88)–(90), respectively.

Next, we discuss the staggered-grid method by dispersion analysis, stability analysis and numerical modeling tests.

Fig. 17 shows the variation of the dispersion parameter δ in Eq. (89) with kh for different space point numbers. Fig. 18 shows 1D stability conditions for the conventional staggered-grid and new staggered-grid methods. Nearly the same conclusions can be drawn from Figs. 17 and 18 as those stated in Sections 4.1 and 5.3. The new staggered-grid FD method has greater accuracy than the conventional staggered-grid FD method and is always stable.

Fig. 19 shows the synthetic seismograms computed by the conventional staggered-grid and the new staggered-grid methods for a homogeneous model. Fig. 20 displays 1D modeling records for an inhomogeneous model. Figs. 19 and 20 also suggest that the new staggered-grid method can adopt a larger time step and obtain more accurate results simultaneously.

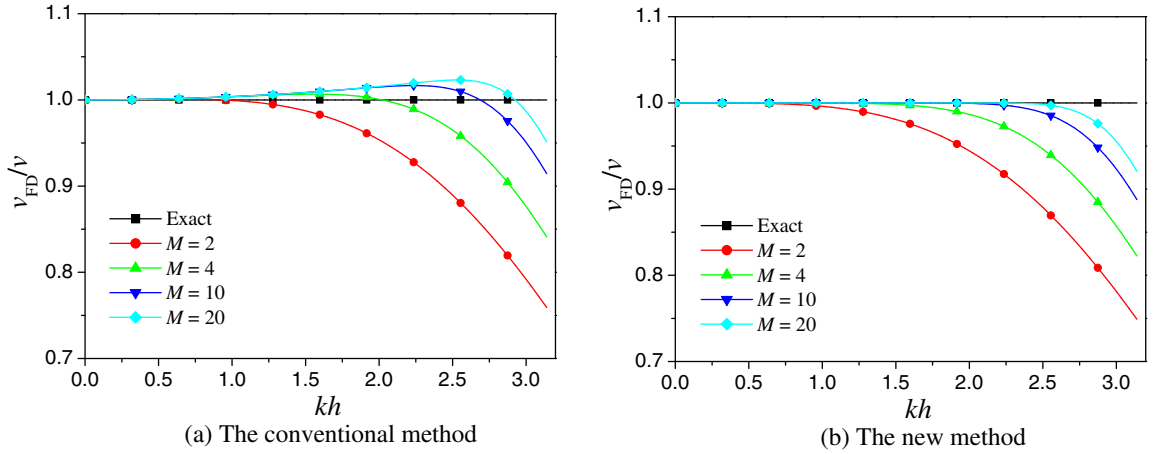

(a) The conventional method (b) The new method

Fig. 17. Plot of 1D dispersion curves of the conventional staggered-grid and the new staggered-grid methods for different space point numbers. $M = 2, 4, 10$ and 20, $v = 3000$ m/s, $\tau = 0.001$ s, $h = 10$ m.

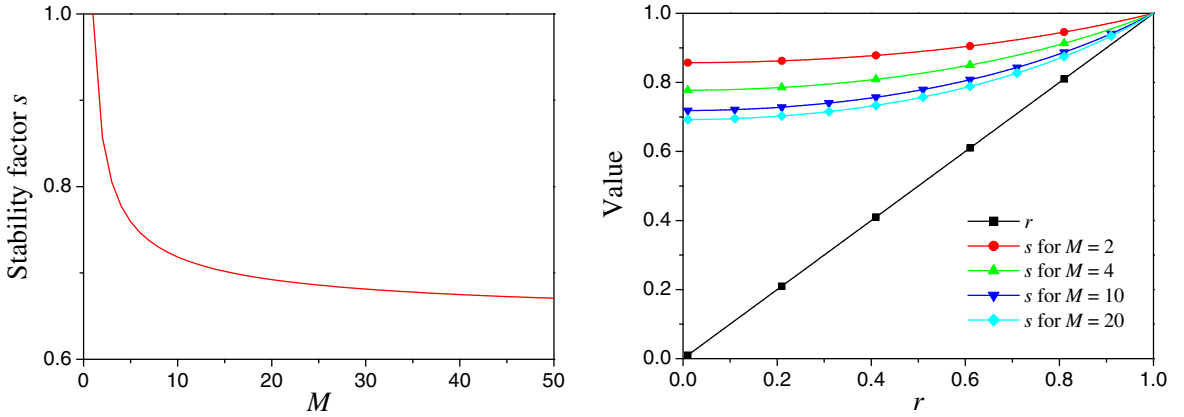

(a) The variation of stability factor s with M for the conventional method

(b) The variation of stability factor s with M and r for the new method.

Fig. 18. Plot of 1D stability conditions for the conventional staggered-grid and the new staggered-grid methods. The method is stable when $r \leqslant s$.

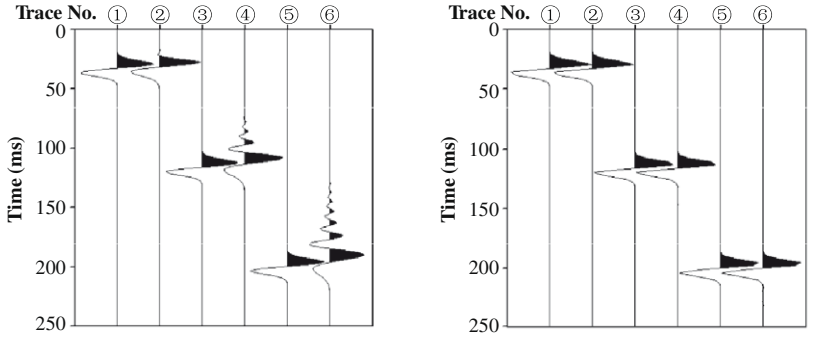

(a) The conventional method, τ=0.002s (b) The new method, τ=0.003s

Fig. 19. 1D modeling records computed by the conventional staggered-grid and the new staggered-grid methods for different time steps. ①, ③ and ⑤ are analytic solutions; ②, ④ and ⑥ are modeling results. Distances between source center and these three receivers are 100, 350 and 600 m, respectively. $\alpha^2 = 1.6$, $v = 3000$ m/s, $h = 10$ m, $M = 20$. The conventional staggered-grid method is unstable when $\tau = 0.003$ s.

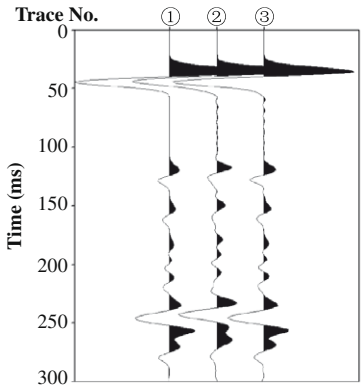

Fig. 20. 1D modeling records computed by the conventional staggered-grid and the new staggered-grid methods for an inhomogeneous model. The model has 10 layers, whose velocities and interfaces' depths are the same as those listed in the caption of Fig. 15. Densities of the 10 layers are 2.0, 2.1, 2.2, 2.3, 2.4, 2.6, 2.8, 2.3, 2.6 and 2.7 g/cm^3, source depth is 100 m, receiver depth is 200 m. $\alpha^2 = 1.5$. ① is the nearly analytic solution, calculated by the 2nd-order staggered-grid method with a very small grid size and time step, that is, $h = 2$ m, $\tau = 0.00025$ s, $M = 1$. Note that for the 2nd-order FD, the new method and the conventional method are the same. ② is calculated by the conventional staggered-grid method, $h = 10$ m, $\tau = 0.0015$ s, $M = 10$. ③ is calculated by the new staggered-grid method, $h = 10$ m, $\tau = 0.002$ s, $M = 10$. The conventional staggered-grid method is unstable when $\tau = 0.002$ s.

8. Conclusions

We have developed a new FD method in time–space domain for the acoustic wave equation based on the methods in [39,40]; the FD coefficients are determined by the Courant number and space point number. The new method has greater accuracy than the conventional method under the same discretization. Also, the new method can adopt a larger time step. Dispersion analysis and numerical modeling results demonstrate that the new method has greater accuracy and can effectively suppress the dispersion and maintain the waveform. We also developed a new time–space domain high-order staggered-grid FD method for the acoustic wave equation with variable densities. This staggered-grid method has similar advantages demonstrated by dispersion analysis, stability analysis and numerical modeling. This method can be extended to solve other similar partial difference equations.

Acknowledgments

We thank the editor Dr. Alvin Bayliss and three anonymous reviewers for constructive criticism of our paper. Liu would like to thank China Scholarship Council for their financial support for this research and UTIG for providing with the facilities. This research is also partially supported by NSFC under Contract No. 40839901, the National "863" Program of China under Contract No. 2007AA06Z218 and KAUST AEA grant at UT Austin.

Appendix A

This appendix gives the derivation of a relation between the calculation amount and the space point number for the 1D acoustic wave equation modeling.

First, we derive the calculation amount of each recursion in the 1D acoustic wave equation modeling. Eq. (5) can be rewritten as follows:

$$p_0^1 = b_0 p_0^0 - p_0^{-1} + \sum_{m=1}^{M} b_m (p_{-m}^0 + p_m^0), \tag{66}$$

where

$$b_0 = 2 + r^2 a_0, \quad b_m = r^2 a_m. \tag{67}$$

Note that the coefficients in (67) can be pre-computed. $2M + 2$ additions or subtractions and $M + 1$ multiplications are involved in the recursion equation (66).

Next, we derive the grid point number and the time step for the 1D acoustic wave modeling. Let $\beta = kh$. From Figs. 1–3, we can see that the modeling accuracy by the new method mainly depends on M when the Courant number r is not very close to zero. For a given positive number η and a given integer number M, there exists a positive real number $\beta_{\max}$ satisfying

$$|\delta - 1| \leqslant \eta \quad \text{when } \beta \leqslant \beta_{\max}. \tag{68}$$

δ is defined by Eq. (49). If all the β values of the wavefield are less than $\beta_{\max}$, the modeling results will have greater accuracy for small value of η. Assuming that λ is the wavenumber and f is the frequency, we have

$$\beta = kh = \frac{2\pi h}{\lambda} = \frac{2\pi h f}{v}. \tag{69}$$

Assume that the maximum frequency of the wavefield is $f_{\max}$, the minimum velocity is $v_{\min}$, then

$$\beta \leqslant \beta_{\max} \quad \text{when } h \leqslant \frac{\beta_{\max} v_{\min}}{2\pi f_{\max}}. \tag{70}$$

We obtain the maximum grid size $h_{\max}$ as

$$h_{\max} = \frac{\beta_{\max} v_{\min}}{2\pi f_{\max}}. \tag{71}$$

Assume that the maximum Courant number used in the modeling is $r_{\max}$. The modeling is stable when $r_{\max} \leqslant 1$. For a given value of $r_{\max}$, the maximum time step $\tau_{\max}$ is given by

$$\tau_{\max} = \frac{h_{\max} r_{\max}}{v_{\min}}. \tag{72}$$

Assume the spatial length and the temporal length in the modeling are L and T, respectively, then the number of grid point n_{h} and the number of time step n_{t} can be expressed as follows:

$$n_{\mathrm{h}} = \frac{L}{h_{\max}} = \frac{2\pi f_{\max} L}{\beta_{\max} v_{\min}}, \tag{73a}$$

$$n_{\mathrm{t}} = \frac{T}{\tau_{\max}} = \frac{v_{\min} T}{h_{\max} r_{\max}} = \frac{2\pi f_{\max} T}{\beta_{\max} r_{\max}}. \tag{73b}$$

Finally, we obtain the relation between the calculation amount and the space point number M. That is, the total multiplication operation times N_{M} and the total addition or subtraction operation times N_{A} are

$$N_{\mathrm{M}} = (M+1) n_{\mathrm{h}} n_{\mathrm{t}} = \frac{4\pi^2 f_{\max}^2 LT}{v_{\min} r_{\max}} \frac{(M+1)}{\beta_{\max}^2}, \tag{74a}$$

$$N_{\mathrm{A}} = 2(M+1) n_{\mathrm{h}} n_{\mathrm{t}} = 2N_{\mathrm{M}}. \tag{74b}$$

Appendix B

This appendix presents the new time–space domain high-order staggered-grid FD method for the 1D acoustic wave equation.

The 1D acoustic wave equation with variable densities is (e.g. [5])

$$\frac{\partial}{\partial x}\left(\frac{1}{\rho}\frac{\partial p}{\partial x}\right) = \frac{1}{K}\frac{\partial^2 p}{\partial t^2}, \tag{75}$$

where ρ is the density, K is the bulk modulus, $K = \lambda + 2\mu = \rho v^2$, v is the velocity, p represents the pressure.

To numerically solve this wave equation, the 2nd-order FD formula (2) is used for the temporal derivative, and the conventional $(2M)$-order staggered-grid FD formula (e.g. [53,42]) for the first-order derivatives is used for the spatial derivatives

$$\frac{\partial p}{\partial x} = \frac{1}{h}\sum_{m=1}^{M} a_m \left(p^0_{m-1/2} - p^0_{-m+1/2}\right), \tag{76}$$

where

$$a_m = \frac{(-1)^{m+1}}{2m-1} \prod_{1 \leqslant n \leqslant M, n \neq m} \left|\frac{(2n-1)^2}{(2n-1)^2 - (2m-1)^2}\right|. \tag{77}$$

It can also be proved that when this $(2M)$th-order space domain staggered-grid FD stencil (76) with FD coefficients (77) and the 2nd-order time domain FD stencil (2) are used to solve the 1D, 2D and 3D acoustic wave equations, the accuracy is of 2nd-order.

Next, we give the new staggered-grid FD method based on the time–space domain dispersion relation. Assuming that the medium is homogeneous and substituting Eqs. (2) and (76) into (75), we have

$$\frac{1}{h^2}\sum_{m=1}^{M}\sum_{n=1}^{M} a_m a_n \left[\left(p^0_{m+n-1} - p^0_{m-n}\right) - \left(p^0_{-m+n} - p^0_{-m-n+1}\right)\right] \approx \frac{1}{v^2\tau^2}\left(p^1_0 + p^{-1}_0 - 2p^0_0\right). \tag{78}$$

Using the plane wave theory, substituting Eq. (6) into (78) and simplifying it, we obtain

$$-\frac{4}{h^2}\left[\sum_{m=1}^{M} a_m \sin((m-0.5)kh)\right]^2 \approx -\frac{4}{v^2\tau^2}[\sin(0.5\omega\tau)]^2, \tag{79}$$

then

$$\sum_{m=1}^{M} a_m \sin((m-0.5)kh) \approx \pm r^{-1}\sin(0.5\omega\tau). \tag{80}$$

When all the a_m are changed to $-a_m$, the final results of FD modeling are the same, we take

$$\sum_{m=1}^{M} a_m \sin((m-0.5)kh) \approx r^{-1}\sin(0.5\omega\tau). \tag{81}$$

Using the Taylor series expansion for sine functions, $r = v\tau/h$ and $\omega = vk$, Eq. (81) can be changes as follows:

$$\sum_{m=1}^{M} a_m \sum_{j=1}^{\infty} \frac{(-1)^{j-1}((m-0.5)kh)^{2j-1}}{(2j-1)!} \approx r^{-1}\sum_{j=1}^{\infty}\frac{(-1)^{j-1}(0.5rkh)^{2j-1}}{(2j-1)!}. \tag{82}$$

Comparing coefficients of k^{2j-1}, we obtain

$$\sum_{m=1}^{M}(2m-1)^{2j-1}a_m = r^{2j-2} \quad (j = 1,2,\ldots,M). \tag{83}$$

We can rewrite Eq. (83) as the following matrix form

$$\begin{bmatrix} 1^0 & 3^0 & \cdots & (2M-1)^0 \\ 1^2 & 3^2 & \cdots & (2M-1)^2 \\ \vdots & \vdots & \vdots & \vdots \\ 1^{2M-2} & 3^{2M-2} & \cdots & (2M-1)^{2M-2} \end{bmatrix} \begin{bmatrix} 1a_1 \\ 3a_2 \\ \vdots \\ (2M-1)a_M \end{bmatrix} = \begin{bmatrix} 1 \\ r^2 \\ \vdots \\ r^{2M-2} \end{bmatrix}. \tag{84}$$

The coefficient matrix of Eqs. (84) is a Vandermonde matrix. Solving these equations, we obtain

$$a_m = \frac{\prod_{1\leqslant n<m}[r^2-(2n-1)^2]\prod_{m<n\leqslant M}[(2n-1)^2-r^2]}{(2m-1)\prod_{1\leqslant n<m}[(2m-1)^2-(2n-1)^2]\prod_{m<n\leqslant M}[(2n-1)^2-(2m-1)^2]} \quad (m = 1,2,\ldots,M). \tag{85}$$

Since it is necessary that $r \leqslant 1$ in numerical modeling, Eq. (85) can be rewritten as

$$a_m = \frac{(-1)^{m+1}}{2m-1}\prod_{1\leqslant n\leqslant M, n\neq m}\left|\frac{(2n-1)^2-r^2}{(2n-1)^2-(2m-1)^2}\right|. \tag{86}$$

When $r = 0$, the FD coefficients are the same as (77) from the conventional method (e.g. [42,53]). That is, the conventional method is just a special case of the new method.

The absolute error can be obtained from Eq. (78) by using (79)

$$\varepsilon = \left|\left[\frac{2}{h}\sum_{m=1}^{M} a_m \sin((m-0.5)kh)\right]^2 - \left[\frac{2}{v\tau}\sin(0.5\omega\tau)\right]^2\right|. \tag{87}$$

With Eqs. (81)–(83), $v = \omega/k$ and $r = v\tau/h$, Eq. (87) can be rewritten as follows:

$$\begin{aligned}\varepsilon &= \left|\left[\frac{2}{h}\sum_{j=1}^{\infty}\left(\sum_{m=1}^{M}(m-0.5)^{2j-1}a_m\right)\frac{(-1)^{j-1}(kh)^{2j-1}}{(2j-1)!}\right]^2 - \left[\frac{2}{v\tau}\sum_{j=1}^{\infty}\frac{(-1)^{j-1}(0.5rkh)^{2j-1}}{(2j-1)!}\right]^2\right| \\ &= \left|\frac{8}{h^2}\left[\sum_{j=1}^{\infty}\frac{(-1)^{j-1}r^{2j-2}(0.5kh)^{2j-1}}{(2j-1)!}\right]\left[\sum_{j=M+1}^{\infty}\left(\sum_{m=1}^{M}(2m-1)^{2j-1}a_m - r^{2j-2}\right)\frac{(-1)^{j-1}(0.5kh)^{2j-1}}{(2j-1)!}\right]\right. \\ &\quad \left. + \left[\frac{2}{h}\sum_{j=M+1}^{\infty}\left(\sum_{m=1}^{M}(m-0.5)^{2j-1}a_m\right)\frac{(-1)^{j-1}(kh)^{2j-1}}{(2j-1)!}\right]^2 - \left[\frac{2}{h}\sum_{j=M+1}^{\infty}\frac{(-1)^{j-1}r^{2j-2}(0.5kh)^{2j-1}}{(2j-1)!}\right]^2\right|.\end{aligned} \tag{88}$$

Since the minimum power of h in the error function is $2M$, the FD accuracy is $(2M)$th-order.

Similar to Eq. (49), we define a parameter δ as follows to describe 1D dispersion of staggered-grid FD

$$\delta = \frac{v_{FD}}{v} = \frac{2}{rkh}\sin^{-1}\left(r\sum_{m=1}^{M} a_m \sin((m-0.5)kh)\right). \tag{89}$$

Using the conventional eigenvalue method of stability analysis, we obtain 1D stability condition as follows:

$$r \leqslant \left(\sum_{m=1}^{M} |a_m|\right)^{-1}. \tag{90}$$

References

[1] K.R. Kelly, R. Ward, W.S. Treitel, R.M. Alford, Synthetic seismograms: a finite-difference approach, Geophysics 41 (1976) 2–27.
[2] S.K. Lele, Compact finite difference schemes with spectral-like resolution, J. Comput. Phys. 103 (1992) 16–42.
[3] J.O.A. Robertsson, J.O. Blanch, W.W. Symes, Viscoelastic finite-difference modeling, Geophysics 59 (1994) 1444–1456.
[4] R. Bansal, M.K. Sen, Finite-difference modelling of S-wave splitting in anisotropic media, Geophys. Prospect. 56 (2008) 293–312.
[5] J.F. Claerbout, Imaging the Earth's Interior, Blackwell Scientific Publications Inc., Palo Alto, CA, 1985.
[6] K. Larner, C. Beasley, Cascaded migrations-improving the accuracy of finite-difference migration, Geophysics 52 (1987) 618–643.
[7] Z. Li, Compensating finite-difference errors in 3-D migration and modeling, Geophysics 56 (1991) 1650–1660.
[8] T. Fei, C.L. Liner, Hybrid Fourier finite difference 3D depth migration for anisotropic media, Geophysics 73 (2008) S27–S34.
[9] J.D. De Basabe, M.K. Sen, M.F. Wheeler, The interior penalty discontinuous Galerkin method for elastic wave propagation: grid dispersion, Geophys. J. Int. 175 (2008) 83–93.
[10] M.A. Dablain, The application of high-order differencing to the scalar wave equation, Geophysics 51 (1986) 54–66.
[11] B. Fornberg, The pseudospectral method – comparisons with finite differences for the elastic wave equation, Geophysics 52 (1987) 483–501.
[12] A. Vafidis, F. Abramovici, E.R. Kanasewich, Elastic wave propagation using fully vectorized high order finite-difference algorithms, Geophysics 57 (1992) 218–232.
[13] C. Liu, Z. Liu, High order finite difference and multigrid methods for spatially evolving instability in a planar channel, J. Comput. Phys. 106 (1993) 92–100.
[14] Y. Liu, C.C. Li, Y.G. Mou, Finite-difference numerical modeling of any even-order accuracy, Oil Geophys. Prospect. 33 (1998) 1–10 (abstract in English).
[15] C. Vanhille, C. Campos-Pozuelo, A high-order finite-difference algorithm for the analysis of standing acoustic waves of finite but moderate amplitude, J. Comput. Phys. 165 (2000) 334–353.
[16] D. You, A high-order Pade ADI method for unsteady convection–diffusion equations, J. Comput. Phys. 214 (2006) 1–11.
[17] J.B. Chen, High-order time discretizations in seismic modeling, Geophysics 72 (2007) SM115–SM122.
[18] J.T. Etgen, M.J. O'Brien, Computational methods for large-scale 3D acoustic finite-difference modeling: a tutorial, Geophysics 72 (2007) SM223–SM230.
[19] Y. Liu, X.C. Wei, Finite-difference numerical modeling with even-order accuracy in two-phase anisotropic media, Appl. Geophys. 5 (2008) 107–114.
[20] R. Madariaga, Dynamics of an expanding circular fault, Bull. Seism. Soc. Am. 66 (1976) 639–666.
[21] J. Virieux, SH-wave propagation in heterogeneous media: velocity-stress finite-difference method, Geophysics 49 (1984) 1933–1957.
[22] J. Virieux, P-SV wave propagation in heterogeneous media: velocity stress finite difference method, Geophysics 51 (1986) 889–901.
[23] K. Yomogida, J.T. Etgen, 3-D wave propagation in the Los Angeles basin for the Whittier-Narrows earthquake, Bull. Seism. Soc. Am. 83 (1993) 1325–1344.
[24] R.W. Graves, Simulating seismic wave propagation in 3D elastic media using staggered-grid finite differences, Bull. Seism. Soc. Am. 86 (1996) 1091–1106.
[25] A. Pitarka, 3D elastic finite-difference modeling of seismic motion using staggered grids with nonuniform spacing, Bull. Seism. Soc. Am. 89 (1999) 54–68.
[26] S. Aoi, H. Fujiwara, 3-D finite-difference method using discontinuous grids, Bull. Seism. Soc. Am. 89 (1999) 918–930.
[27] R. Mittet, Free-surface boundary conditions for elastic staggered-grid modeling schemes, Geophysics 67 (2002) 1616–1623.
[28] O. Rojas, S. Day, J. Castillo, L.A. Dalguer, Modelling of rupture propagation using high-order mimetic finite differences, Geophys. J. Int. 172 (2008) 631–650.
[29] E.H. Saenger, N. Gold, S.A. Shapiro, Modeling the propagation of elastic waves using a modified finite-difference grid, Wave Motion 31 (2000) 77–92.
[30] E.H. Saenger, S.A. Shapiro, Effective velocities in fractured media: a numerical study using the rotated staggered finite difference grid, Geophys. Prospect. 50 (2002) 183–194.
[31] E.H. Saenger, T. Bohlen, Finite-difference modeling of viscoelastic and anisotropic wave propagation using the rotated staggered grid, Geophysics 69 (2004) 583–591.
[32] O.S. Krüger, E.H. Saenger, S. Shapiro, Scattering and diffraction by a single crack: an accuracy analysis of the rotated staggered grid, Geophys. J. Int. 162 (2005) 25–31.
[33] S. Emerman, W. Schmidt, R. Stephen, An implicit finite-difference formulation of the elastic wave equation, Geophysics 47 (1982) 1521–1526.
[34] D. Ristow, T. Ruhl, 3-D implicit finite-difference migration by multiway splitting, Geophysics 62 (1997) 554–567.
[35] J.A. Ekaterinaris, Implicit, high-resolution, compact schemes for gas dynamics and aeroacoustics, J. Comput. Phys. 156 (1999) 272–299.
[36] T. Nihei, K. Ishii, A fast solver of the shallow water equations on a sphere using a combined compact difference scheme, J. Comput. Phys. 187 (2003) 639–659.
[37] S.E. Sherer, J.N. Scott, High-order compact finite-difference methods on general overset grids, J. Comput. Phys. 210 (2005) 459–496.
[38] Z.F. Tian, S.Q. Dai, High-order compact exponential finite difference methods for convection–diffusion type problems, J. Comput. Phys. 220 (2007) 952–974.
[39] B. Finkelstein, R. Kastner, Finite difference time domain dispersion reduction schemes, J. Comput. Phys. 221 (2007) 422–438.
[40] B. Finkelstein, R. Kastner, A comprehensive new methodology for formulating FDTD schemes with controlled order of accuracy and dispersion, IEEE Trans. Antenna Propagat. 56 (2008) 3516–3525.
[41] Y. Liu, M.K. Sen, A practical implicit finite-difference method: examples from seismic modeling, J. Geophys. Eng. 6 (2009) 231–249.
[42] Y. Liu, M.K. Sen, An implicit staggered-grid finite-difference method for seismic modeling, Geophys. J. Int. doi:10.1111/j.1365-246X.2009.04305.x.
[43] B. Fornberg, Calculation of weights in finite difference formulas, SIAM Rev. 40 (1998) 685–691.
[44] O. Holberg, Computational aspects of the choice of operator and sampling interval for numerical differentiation in large-scale simulation of wave phenomena, Geophys. Prospect. 35 (1987) 625–655.
[45] C. Jastram, A. Behle, Accurate finite-difference operators for modelling the elastic wave equation, Geophys. Prospect. 41 (1993) 453–458.
[46] C.K.W. Tam, J.C. Webb, Dispersion-relation-preserving finite difference schemes for computational acoustics, J. Comput. Phys. 107 (1993) 262–281.
[47] R. Hixon, Nonlinear comparison of high-order and optimized finite-difference schemes, Int. J. Comput. Fluid Dynam. 13 (2000) 259–277.

[48] C. Bogey, C. Bailly, A family of low dispersive and low dissipative explicit schemes for flow and noise computations, J. Comput. Phys. 194 (2004) 194–214.
[49] R.J. Geller, N. Takeuchi, A new method for computing highly accurate DSM synthetic seismograms, Geophys. J. Int. 123 (1995) 449–470.
[50] N. Takeuchi, R.J. Geller, P.R. Cummins, Highly accurate P-SV complete synthetic seismograms using modified DSM operators, Geophys. Res. Lett. 23 (1996) 1175–1178.
[51] N. Takeuchi, R.J. Geller, Optimally accurate second order time-domain finite difference scheme for computing synthetic seismograms in 2-D and 3-D media, Phys. Earth Planet. Int. 119 (2000) 99–131.
[52] A. JafarGandomi, H. Takenaka, Non-standard FDTD for elastic wave simulation: two-dimensional P-SV case, Geophys. J. Int. 178 (2009) 282–302.
[53] M. Kindelan, A. Kamel, P. Sguazzero, On the construction and efficiency of staggered numerical differentiators for the wave equation, Geophysics 55 (1990) 107–110.